

NON-LINE-OF-SIGHT ELECTRO-OPTIC
LASER COMMUNICATIONS IN THE
MIDDLE ULTRAVIOLET.

Dennis Michael Junge

NAVAL POSTGRADUATE SCHOOL

Monterey, California



THESIS

NON-LINE-OF-SIGHT ELECTRO-OPTIC LASER
COMMUNICATIONS IN THE MIDDLE ULTRAVIOLET

by

Dennis Michael Junge

December 1977

Thesis Advisor:

W.M. Tolles

Approved for public release; distribution unlimited.

Prepared for:

Naval Weapons Center
China Lake, California

T181455

NAVAL POSTGRADUATE SCHOOL
Monterey, California

Rear Admiral Isham Linder
Superintendent

Jack R. Borsting
Provost

This thesis prepared in conjunction with research supported in part by Naval Weapons Center, China Lake, California, under project number N6053077WR30252.

Reproduction of all or part of this report is authorized.

REPORT DOCUMENTATION PAGE		READ INSTRUCTIONS BEFORE COMPLETING FORM
1. REPORT NUMBER NPS61-77-001	2. GOVT ACCESSION NO.	3. RECIPIENT'S CATALOG NUMBER
4. TITLE (and Subtitle) Non-Line-of-Sight Electro-Optic Laser Communications in the Middle Ultraviolet		5. TYPE OF REPORT & PERIOD COVERED Master's Thesis; December 1977
		6. PERFORMING ORG. REPORT NUMBER
7. AUTHOR(s) Dennis Michael Junge in conjunction with William M. Tolles		8. CONTRACT OR GRANT NUMBER(s)
9. PERFORMING ORGANIZATION NAME AND ADDRESS Naval Postgraduate School Monterey, California 93940		10. PROGRAM ELEMENT, PROJECT, TASK AREA & WORK UNIT NUMBERS 62332N; 32342 N6053077WR30252
11. CONTROLLING OFFICE NAME AND ADDRESS Naval Postgraduate School Monterey, California 93940		12. REPORT DATE December 1977
		13. NUMBER OF PAGES 100
14. MONITORING AGENCY NAME & ADDRESS (if different from Controlling Office)		15. SECURITY CLASS. (of this report) Unclassified
		15a. DECLASSIFICATION/DOWNGRADING SCHEDULE
16. DISTRIBUTION STATEMENT (of this Report) Approved for public release; distribution unlimited.		
17. DISTRIBUTION STATEMENT (of the abstract entered in Block 20, if different from Report)		
18. SUPPLEMENTARY NOTES		
19. KEY WORDS (Continue on reverse side if necessary and identify by block number) Electro-optic laser communication middle ultraviolet multiple scattering non-line-of-sight		
20. ABSTRACT (Continue on reverse side if necessary and identify by block number) A Monte Carlo computer simulation was developed to model hypothesized electro-optic laser communication systems operating in the middle ultraviolet region of the spectrum called the solar blind. By assuming various source, propagation, and detector characteristics as well as certain performance parameters it is possible to predict the effective ranges and operating characteristics		

UNCLASSIFIED

SECURITY CLASSIFICATION OF THIS PAGE(When Data Entered)

(20. ABSTRACT Continued)

of such a system.

UNCLASSIFIED

Approved for public release; distribution unlimited.

Non-Line-of-Sight Electro-Optic Laser
Communications in the Middle Ultraviolet

by

Dennis Michael Junge
Lieutenant, United States Navy

Submitted in partial fulfillment of the
requirements for the degree of

MASTER OF SCIENCE IN APPLIED SCIENCE

from the

NAVAL POSTGRADUATE SCHOOL

December 1977

2.1
ABSTRACT

A Monte Carlo computer simulation was developed to model hypothesized electro-optic laser communication systems operating in the middle ultraviolet region of the spectrum called the solar blind. By assuming various source, propagation, and detector characteristics as well as certain performance parameters it is possible to predict the effective ranges and operating characteristics of such a system.

ACKNOWLEDGMENTS

The authors would like to express their appreciation to Dr. Michael E. Neer, Aeronautical Research Associates of Princeton (ARAP), Princeton, New Jersey; Dr. Nicholas M. Uros, Pacific Missile Range, Point Mugu, California; and Dr. Alexander S. Zachor, Honeywell, Inc. Radiation Center, Lexington, Massachusetts, for their interest in and contributions to this project.

TABLE OF CONTENTS

I.	INTRODUCTION -----	10
	A. HISTORY -----	10
	B. VISIBLE LIGHT -----	11
	C. INFRARED LIGHT -----	11
	D. ULTRAVIOLET LIGHT -----	12
	E. PURPOSE -----	13
II.	BACKGROUND -----	14
	A. INTRODUCTION -----	14
	B. SOURCES -----	15
	C. PROPAGATION -----	16
	D. DETECTION/DEMODULATION -----	18
III.	STATEMENT OF THE PROBLEM -----	19
IV.	LASER SOURCES -----	21
V.	PROPAGATION PROPERTIES OF THE ATMOSPHERE AND THE MULTIPLE SCATTERING PROBLEM -----	23
	A. INTRODUCTION -----	23
	B. CHARACTERISTICS OF THE ATMOSPHERE -----	23
	1. Attenuation -----	23
	2. Angular Distribution of Scattered Photons -----	24
	C. DESCRIPTION OF THE CHARACTERISTICS OF THE SIMULATION -----	31
	D. CHARACTERISTIC PATTERNS OF MULTIPLY SCATTERED RADIATION -----	32
	E. FIELD OF VIEW CONSIDERATIONS -----	40
	F. PULSE SPREADING CONSIDERATIONS -----	43
	G. SUMMARY -----	46

VI.	SIGNAL-TO-NOISE CONSIDERATIONS -----	47
A.	INTRODUCTION -----	47
B.	FUNDAMENTAL RELATIONSHIPS -----	47
C.	BACKGROUND LEVEL OF RADIATION -----	49
D.	DETECTOR CHARACTERISTICS -----	50
E.	STATISTICAL CONSIDERATIONS -----	51
F.	SUMMARY OF SIGNAL-TO-NOISE CONSIDERATIONS ---	53
VII.	DISCUSSION -----	55
VIII.	CONCLUSIONS -----	58
APPENDIX A:	MONTE CARLO SIMULATION OF THE MULTIPLE SCATTERING PROBLEM -----	59
APPENDIX B:	DEVELOPMENT OF THE FUNDAMENTAL RELATIONSHIP FOR RAYLEIGH SCATTERING -----	68
APPENDIX C:	SAMPLE CALCULATION FOR RANGE PREDICTION --	71
APPENDIX D:	CHECKS ON POSSIBLE ERRORS -----	73
APPENDIX E:	PROGRAM DESCRIPTION AND DOCUMENTATION ----	75
	COMPUTER PROGRAM -----	79
	LIST OF REFERENCES -----	97
	INITIAL DISTRIBUTION LIST -----	100

LIST OF TABLES

TABLE I.	Characteristic Wavelengths of Several Rare Gas-Halide Lasers Along with Some Stokes Shifted Wavelengths Observed with Hydrogen Gas -----	22
TABLE II.	Attenuation Coefficients and Charac- teristic Ratios for Middle UV Radiation ----	25
TABLE III.	Coefficients Used in the Simulation -----	30
TABLE IV.	Photon Flux Due to Direct and Diffuse Transmittance through the Earth's Atmosphere [12] -----	50
TABLE V.	Photon Flux Required in order to Give a S/N Equal to Ten -----	54
TABLE VI.	Predicted Ranges or Range Bands for Communication in the Middle UV for Pulsed Millijoule Lasers (Simulation) -----	56

LIST OF FIGURES

FIGURE 1	Absolute Phase Function vs. Scattering Angle [23] -----	26
FIGURE 2	Absolute Phase Function vs. Scattering Angle Utilizing a Modified Henyey- Greenstein Function to Approximate the Data by Neer, et al. [23] -----	28
FIGURE 3	Normalized Phase Function vs. Scattering Angle Utilizing a Modified Henyey- Greenstein Function to Approximate the Data by Neer, et al. [23] -----	29
FIGURES 4-7	Photon Scattering Diagram (θ' vs ϕ') as Viewed by a Receiver Located θ Degrees from the Axis of Propagation -----	33
FIGURES 8-10	Contours of Equal Photon Flux as a Function of the Position of the Observer ---	37
FIGURES 11-12	Relative Number of Photons vs Field of View for an Observer Located θ Degrees from the Axis of Propagation -----	41
FIGURES 13-14	Pulse spreading for an Observer Located θ Degrees from the Axis of Propagation -----	44
FIGURE 15	Transmission Characteristics for a Typical Composite Filter -----	52
FIGURE 16	Diagram of the Photon Fixed Coordinate System -----	63

I. INTRODUCTION

A. HISTORY

Historically optical communications systems were developed over line-of-sight paths due to the propagation characteristics of light. In the United States Navy line-of-sight communications became somewhat neglected with the advent of uhf radio technology. For years the only optical communication systems in the navy were the 12 inch (and for a time 24 inch) hand modulated signal lamps, yardarm blinkers, flag hoist, semaphore, and NANCY (a hand modulated infrared system). Some experimentation was conducted in the late 1940's and 1950's using cesium lamps operating in the near infrared (ir) and non-line-of-sight or over-the-horizon (OTH) communication was demonstrated. Interest waned, however, and progress stood still.

Technology has not stood still and today virtually any radio signal can be monitored and the transmitter localized using a direction finding receiver. While communication systems must be reliable and secure, sometimes it is important that they be covert (only detectable by friendly forces). Thus armed with a complete set of radio communication equipment, the unit commander nevertheless may find his forces in EMCON, talking to each other via flashing light.

B. VISIBLE LIGHT

In the 1960's several attempts were again made to demonstrate the feasibility of OTH and over-terrestrial-obstacles communication using atmospheric scattering [1-3]. These efforts utilized visible search lights, flash lamps, and lasers, and communication at night was successfully demonstrated over distances up to fifty kilometers.

Visible radiation is highly attractive because of the low extinction coefficients (depending on weather conditions). Unfortunately it is seriously degraded during daylight hours due to the background radiation from the sun which tends to interfere with detection.

C. INFRARED LIGHT

Recently, efforts have been made to study extended line-of-sight communications utilizing lasers operating in the near ir. One such effort utilized a 1.06 μ laser and employed remotely piloted vehicles (RPVs). Communications at this wavelength appeared quite promising and ranges from 25 to 150 nautical miles have been predicted [4].

In this region of the spectrum, however, there is noticeable background noise due to scattering of incident solar radiation and to emission by atmospheric particles heated by incident radiation. It should be noted that the daylight background visible radiance is due primarily to scattered radiation and night radiance is caused mainly by scattered radiation and moon light. In the near ir daylight

background radiance is due mainly to atmospheric emission, while at night aurora and afterglow are the predominate sources.

D. ULTRAVIOLET LIGHT

There is a portion of the spectrum, however, that has been studied little and may offer much. This is the middle ultraviolet (uv). Atmospheric absorption in the .2 to .3 μ region is caused primarily by ozone [5-6]. The relatively dense layer of ozone (at approximately 22 km) prevents virtually all of the radiation in the 220 to 280 nm region from reaching the surface of the earth. Thus the limiting noise in an electro-optical communication system operating in the middle uv would be self-noise rather than atmospheric noise. Another critical feature to be considered is the attenuation properties of the intervening atmosphere. In the near uv (wavelengths between .3 and .4 μ) the primary attenuation mechanism at low altitude is scattering. This can be divided into Rayleigh scattering and particulate scattering by atmospheric aerosols. Rayleigh scattering, inversely proportional to the fourth power of wavelength, increases quite rapidly as the wavelengths become shorter. In practice, it has been difficult to determine the particulate scattering in the near uv. For clear sky conditions, however, a reasonable estimate of attenuation can be made by assuming that the entire attenuation is due to Rayleigh scattering [2].

In the middle uv particulate scattering is very significant. At high altitudes the large ozone concentration

gives rise to very large absorption coefficients. The concentration of ozone generally decreases as the altitude is decreased. Yet even at sea level the concentration is still high enough to have a significant effect. These propagation characteristics indicate that only short range communication systems operating in the middle uv are likely to be useful. Because of the inherent scattering characteristics of middle uv radiation, along with the minimal background problem in the solar blind region, short range non-line-of-sight communications utilizing broad band light sources have been developed [7-8].

Recently a number of reasonably efficient uv lasers have been developed with energies of .1 to one joule per pulse being reported [9-10]. These represent a new generation of radiation sources to be considered for use in the solar blind. A number of detectors and filters have been available for some time. It was these considerations that led to this study.

E. PURPOSE

The purpose of this effort is to develop an analytical tool for estimating the ranges for which optical communication is possible in the middle uv.

II. BACKGROUND

A. INTRODUCTION

A typical communication system consists of a transmitter, a receiver, and the intervening space between them. The characteristics of the transmitter and the receiver are highly dependent on each other and on the properties of the propagating medium. Each of the components may, however, be treated as a distinct and relatively separate entity. The radiation source, or transmitter, must be suitably modulated to carry information and must have sufficient power to overcome the attenuating mechanisms in the medium in which it operates. The characteristics of the propagating medium are not well defined and in general must be approximated. The detector, or receiver, must have sufficient sensitivity to detect and demodulate the attenuated signal that is embedded in background noise. Each of these components is present in an electro-optical communication system and is discussed below. It will be seen that

- 1) advances in sources dictate a new look at the problem;
- 2) uncertainties in propagation characteristics of the middle uv requires careful experimentation to gather suitable information such that a proposed system may be modeled; and
- 3) certain aspects of detectors, such as filters, critically determine the performance parameters of such a system.

B. SOURCES

Ultraviolet sources suitable for communication purposes include omnidirectional broad band lamps such as xenon or mercury flash lamps, and lasers. Experiments utilizing omnidirectional sources have been carried out for several years at the Aeronautical Research Associates of Princeton (ARAP), Princeton, New Jersey [7-8]. Utilizing a pulsed source at 4810 pps and an average power level of ten to thirty watts, voice communication was demonstrated over a distance of several hundred meters. With suitable modifications, it is estimated that ranges of up to three kilometers may be achieved with the current system. With such a source, the conversion efficiency from input power to output power is about 0.1 percent.

New uv laser sources reported in the last year or so appear to have demonstrated orders of magnitude improvement in efficiency. Utilizing rare gas-halide eximer species, uv output with working efficiencies of up to ten percent are conceivable. Practical working models are already commercially available. Wavelengths in the range of 200 to 400 nm have been reported, indicating that various wavelengths in the middle uv may be attained with these sources. The power output of these devices typically runs from 0.1 joules upwards, depending on the size of the device. The high degree of collimation of the output suggests that the geometric patterns for communication will be highly directional. This is one aspect of the problem which is quite different from that observed for omnidirectional sources.

C. PROPAGATION

The absorption coefficient for middle uv radiation varies by orders of magnitude as a function of wavelength. Scattering by particulates at these wavelengths is more severe than in the visible region of the spectrum. The combined absorption and scattering cross-sections give rise to extinction coefficients which have been measured to be in the range of 0.1 to five per kilometer [11]. Further, variations of an order of magnitude in extinction coefficient over a spectral range of less than fifty nanometers indicates extreme sensitivity to wavelength, due largely to the absorption bands of species such as ozone which appear in this region.

At wavelengths less than 280 nm, the absorption coefficient of atmospheric ozone is sufficiently intense as to eliminate the large majority of solar radiation from the earth's surface [12]. This is largely due to an ozone concentration centered at 20 to 25 km above the surface of the earth. At sea level, the ozone concentration is typically an order of magnitude less than at the higher altitudes. This gives rise to reduced solar background levels without the high extinction coefficients found at higher altitudes. Such behavior suggests that communication in the middle uv may be feasible for relatively short distances at sea level, with a minimum of interference from solar background radiation.

Further major considerations for middle uv propagation are the effects due to multiple scattering. Although the primary light beam may be attenuated by an extinction coefficient which is readily measured, the scattered radiation, especially after multiple scattering, may contribute considerable intensity to the radiation density at an observer. Shettle and Green [12] present calculations for solar flux as a function of the sun's angle with respect to the zenith. Particularly at low angles of incidence, the diffuse radiation is found to be twenty to thirty orders of magnitude more intense than that due to the direct solar radiation. Such figures clearly emphasize the importance of properly treating the effects of multiple scattering when taking into account the effects of particulates in the atmosphere.

In general multiple scattering calculations are cumbersome to handle and yield limited information. Typically these calculations are done on a computer using either an analytical [13] or a Monte Carlo [14-15] approach. The Monte Carlo calculations are relatively easier to model, but utilize a significant amount of computer time and only approximate information is obtained. Some generally useful results have been presented by Bucher [14-15] again indicating orders of magnitude greater radiation densities from the multiple scattering effects than from transmission of direct radiation. The available results from such calculations do not readily answer questions such as 1) what is the

scattering intensity for non-line-of-sight communication given an obstacle with an assumed angle between transmitter-obstacle-receiver; and 2) what is the actual radiation density as a function of field of view and/or position of an observer located off from the axis of propagation at a given distance from a collimated source such as a laser.

D. DETECTION/DEMODULATION

The information available from a pulsed signal depends on the pulse width, repetition rate, and signal-to-noise ratio. Considerations such as these are included in papers by Kennedy [16-17] in which communication through optical scattering channels is discussed. Considerations leading to a suitable signal-to-noise ratio analysis are also presented by Yarif [18] for electro-optical systems. Whether the information is pulsed or continuous wave greatly affects the reception characteristics of the signal. The background light levels coming through the filters utilized before the detector critically determine the signal-to-noise ratio. The characteristics of the filter and detector thus are crucial in determining the information available in a communication system.

III. STATEMENT OF THE PROBLEM

One of the primary constraints on the development and deployment of any new system in the United States Navy is the limited fiscal resources available for such efforts. With the advent of new technology it is nevertheless impossible to utilize the technology to build a new system without first having a mission or demonstrated need for that system and second having a well-defined degree of confidence in the ability of that system to meet that need.

An electro-optical communication system utilizing a laser operating in the middle uv is such a system. (It requires little or no imagination to visualize the advantages of rapid short range, possibly non-line-of-sight, optical communications over the methods presently employed by the Fleet.) While it is beyond the scope of this project to develop such a system, it is within the scope of this effort to formulate a model of such a system capable of predicting the various parameters of that system.

The need for modeling is further enhanced by the limited amount of information available concerning the middle uv. By utilizing available information and by characterizing source, propagation, filter and detector characteristics, it is possible to formulate a model that will yield order of magnitude results for any proposed system. In the process of modeling and analysis the need for critical experiments

which would allow the modeling efforts to proceed with a greater degree of accuracy is sure to be revealed.

IV. LASER SOURCES

The past two or three years have seen a rapid development of lasers operating in the ultraviolet. The most notable recent advances have occurred with the rare gas-halide lasers in which an excited state eximer is formed. With species such as XeF^* , the ground state is not an associated molecule, thus depopulation of the lower level is not a barrier to population inversion. Further, such rare gas-halide lasers have an inherently high quantum efficiency. Efficiencies relative to the energy deposited by an excitation electron beam are as high as ten percent, while overall working efficiencies of up to one percent have been reported [9,10,19]. With higher overall efficiencies anticipated, such lasers represent an attractive source of radiation for middle uv applications.

The observed wavelengths of several rare gas-halide lasers are presented in Table I. It should be noted that the laser output from these sources may be Raman shifted with reasonable high conversion efficiencies [20]. By passing the output from a KrF laser through ten atmospheres of hydrogen, conversion to the first stokes wavelength of 25 percent and to the second stokes wavelength of ten percent was observed [20]. At eighty atmospheres pressure, more than fifty percent conversion efficiency to the first stokes wavelength has been observed.

TABLE I

Characteristic Wavelengths of Several Rare
Gas-Halide Lasers Along with Some Stokes
Shifted Wavelengths Observed with Hydrogen Gas

<u>Eximer</u>	<u>Wavelength (nm)</u>	<u>First Stokes Wavelength (nm)</u>	<u>Second Stokes Wavelength (nm)</u>
KrF	249	279	318
XeF	351		
XeCl	308		
XeBr	282	322	

The practical performance of rare gas-halide lasers is illustrated by the commercial availability of a model which will produce 0.1 joule pulses at 15 pps. One table top model is reported to produce 1.5 joule pulses with a 125 nanosecond pulse width. The development of these lasers is in its infancy. Sources with higher repetition rates and greater reliability are to be expected.

Due to the rapidly expanding availability of middle uv lasers sources, no single presently available source is assumed, but rather the effort in the succeeding sections considers the possibility of utilizing a middle uv source at representative wavelengths and with an output power consisting of millijoule to joule pulses. Thus the behavior of any unforeseen laser or coherent beam may be predicted.

V. PROPAGATION PROPERTIES OF THE ATMOSPHERE AND THE MULTIPLE SCATTERING PROBLEM

A. INTRODUCTION

A laser signal propagating through the atmosphere is subjected to various attenuation mechanisms. The time spread of a pulse can be broadened due to scattering, while the amplitude can be decreased due to absorption and scattering by atmospheric constituents. The inherent directionality of a laser source indicates that the position of the detector relative to the source should also affect the reception of the signal. Since a large fraction of the total extinction process is due to scattering, multiple scattering should be an important consideration affecting the propagation characteristics for distances greater than one or two extinction lengths.

A complete description of all of the effects of the atmosphere including inhomogeneities (clouds, terrestrial objects, surface effects, etc.) is beyond the scope of this paper. A relatively concise treatment of the atmosphere and the multiple scattering problem entails characterizing the atmosphere, simulating atmospheric effects, and tabulating the results of the simulation.

B. CHARACTERISTICS OF THE ATMOSPHERE

1. Attenuation

In order to characterize the propagation of optical information in the atmosphere it was first necessary to

determine the extinction, absorption, and scattering coefficients. Table II was constructed based primarily on the information reported by Dunkelman [21]. The Rayleigh scattering coefficients were adapted from Penndorf [22].

For the purpose of this investigation the following definitions and relationships apply:

λ is the wavelength

K_A is the absorption coefficient

K_{SR} is the Rayleigh scattering coefficient

K_{SP} is the particulate scattering coefficient

K_S is the total scattering coefficient

K is the total extinction coefficient

$$K_S = K_{SR} + K_{SP}$$

$$K = K_S + K_A$$

R_S is the ratio of K_S to K or (K_S/K)

R_P is the ratio of K_{SP} to K_S or (K_{SP}/K_S)

From Table II it can be seen that K_A , K_{SR} , and K tend to decrease as wavelength increases in the middle uv. The relationship of K_{SP} and consequently K_S , R_S , and R_P to wavelength is not so easily described.

2. Angular Distribution of Scattered Photons

Complete characterization of the propagation of optical information required the angular distribution or phase function, $P(\theta)$, of the scattered photons for the wavelengths of interest. Figure 1 [23] was the primary source for phase function information.

TABLE II

Attenuation Coefficients and Characteristic Ratios
for Middle uv Radiation

λ (nm)	K_A (km^{-1})	K_{SR} (km^{-1})	K_{SP} (km^{-1})	K_S (km^{-1})	K (km^{-1})	R_S (K_S/K)	R_P (K_{SP}/K_S)
230	2.58-3.5	.4934	.03-2.9	.52-3.4	3.1-6.0	.17-.57	.06-.85
240	1.43-2.8	.4061	.26-3.2	.67-3.6	2.1-5.0	.32-.72	.39-.89
250	.68-2.6	.3382	.18-2.4	.52-2.7	1.2-3.4	.43-.79	.35-.89
260	.43-2.4	.2842	.29-2.2	.57-2.5	1.0-2.9	.57-.86	.51-.88
270	.23-1.6	.2404	.33-2.1	.57-2.3	.80-2.6	.71-.88	.58-.91
280	.13-.89	.2055	.065-1.9	.27-2.1	.40-2.2	.68-.95	.24-.90
290	.046-.32	.1765	.078-1.9	.25-2.1	.30-2.1	.83-1.00	.31-.90
300	.012-.081	.1525	.056-1.7	.21-1.9	.22-1.9	.95-1.00	.27-.89
310	.003-.021	.1326	.044-1.6	.17-1.7	.18-1.8	.94	.26-.94

ABSOLUTE PHASE FUNCTION vs SCATTERING ANGLE

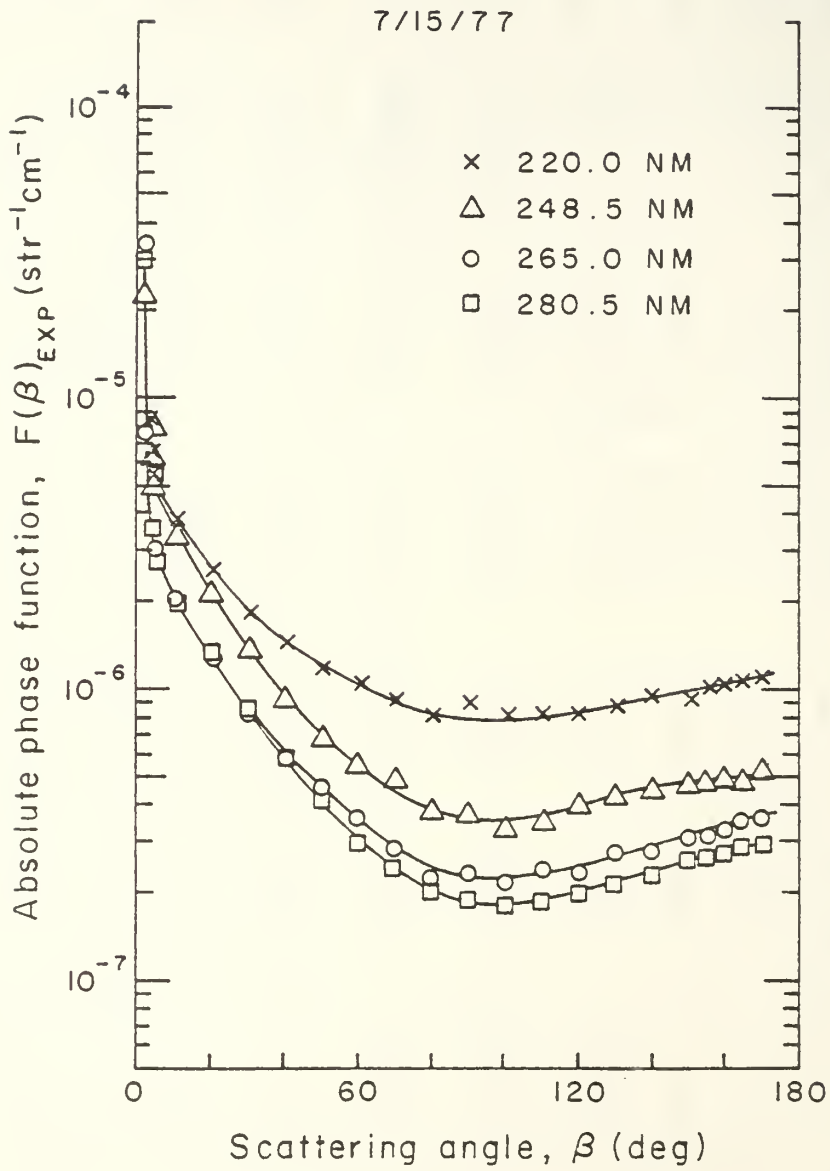


FIGURE 1. Absolute Phase Function vs. Scattering Angle [23]

In order to mathematically model this information, the Henyey-Greenstein function, Eq. 1, and some of its modifications were studied. The Neer-Sandri function [7], Eq. 2, was a logical choice; however, the function used by Zachor [24], Eq. 3, was chosen for simplicity in modifying the author's initial phase function to properly account for backscattering.

$$P(\theta, g) = \frac{1-g^2}{4\pi} \left[\frac{1}{(1+g^2-2g \cos \theta)^{3/2}} \right] \quad (1)$$

$$P(\theta, g) = \frac{1-g^2}{4\pi} \left[\frac{1}{(1+g^2-2g \cos \theta)^{3/2}} + \frac{g(3 \cos^2 \theta - 1)}{2 |\cos \theta_0| (1+g^2-2g |\cos \theta_0|)^{5/2}} \right] \quad (2)$$

$$\text{where } |\cos \theta_0| = 1/7$$

$$P(\theta, g) = \frac{1-g^2}{4\pi} \left[\frac{1}{(1+g^2-2g \cos \theta)^{3/2}} + \frac{f 0.5(3 \cos^2 \theta - 1)}{(1+g^2)^{3/2}} \right] \quad (3)$$

Fitting the data reported by Neer [23] with Eq. 3 resulted in Figures 2 and 3. These figures represent the absolute and normalized phase functions, while Table III lists the coefficients, utilized for this simulation.

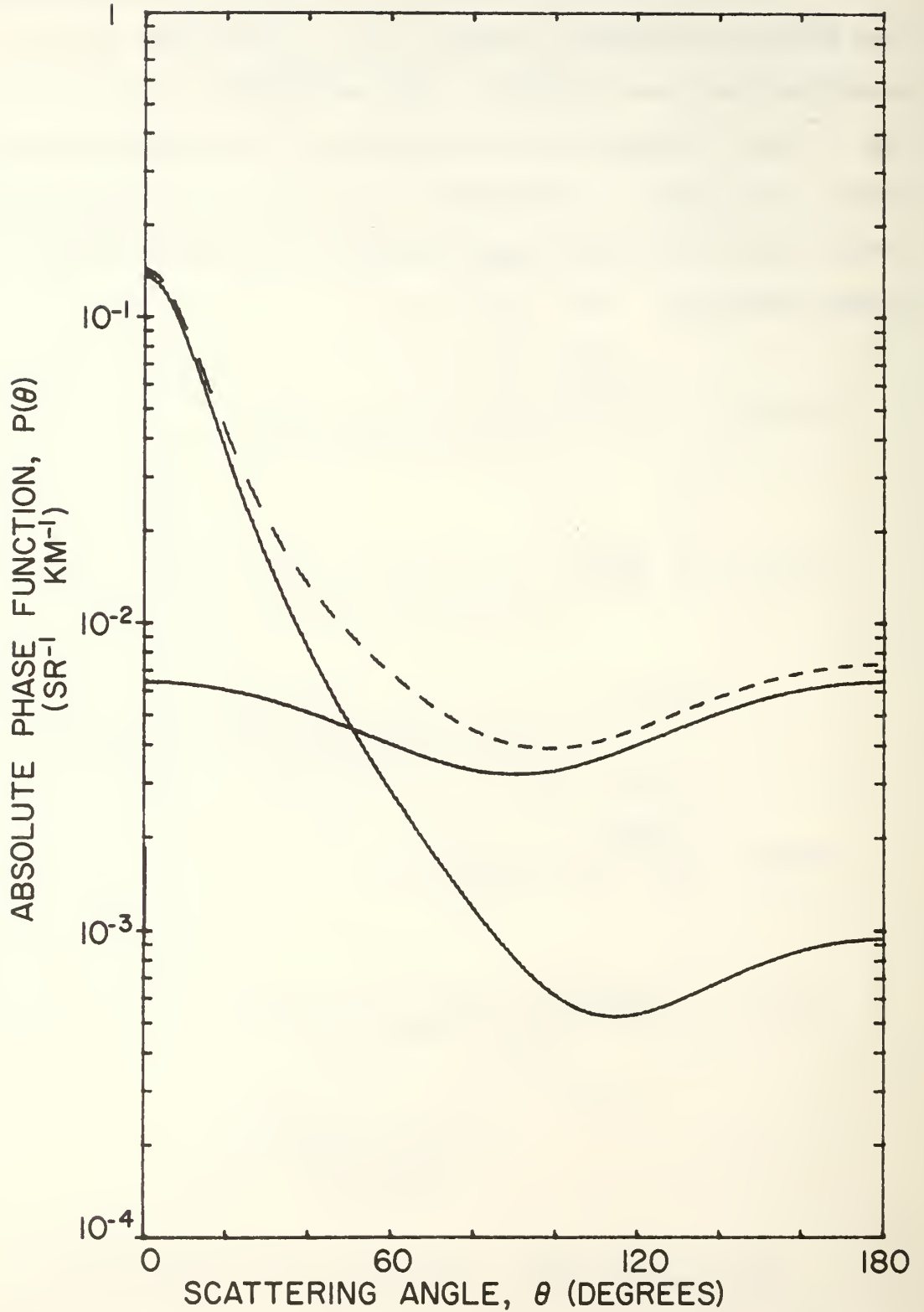


FIGURE 2. Absolute Phase Function vs. Scattering Angle Utilizing a Modified Henyey-Greenstein Function to Approximate the Data by Neer, et al. [23]

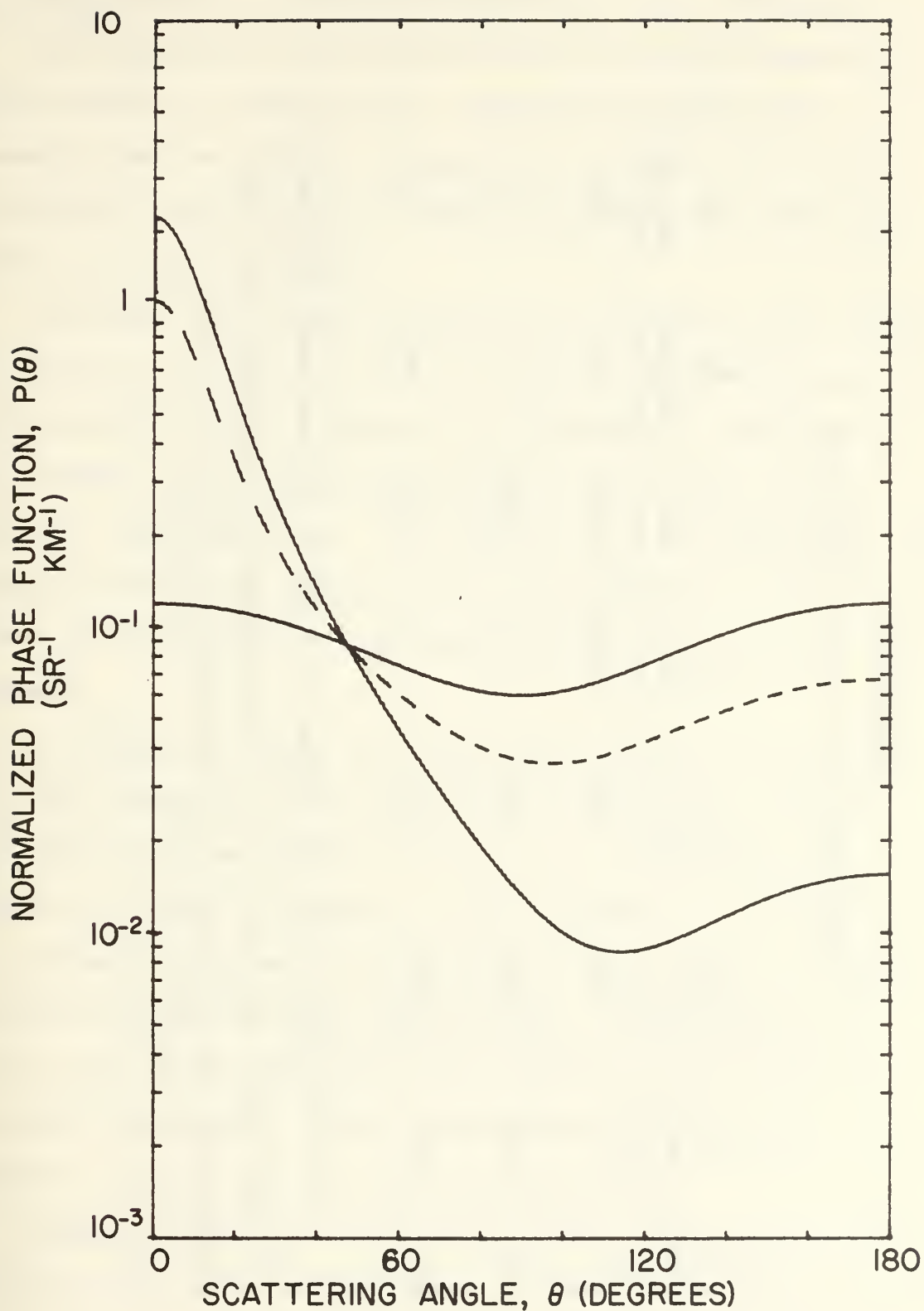


FIGURE 3. Normalized Phase Function vs. Scattering Angle Utilizing a Modified Henyey-Greenstein Function to Approximate the Data by Neer, et al. [23]

TABLE III
Coefficients Used in the Simulation

λ (nm)	K_A (km^{-1})	K_{SR} (km^{-1})	K_{SP} (km^{-1})	K_S (km^{-1})	K (km^{-1})	R_S (K_S/K)	R_P (K_{SP}/K_S)
250	.9372	.3382	.7187	1.0569	1.9941	.53	.68
280	.2185	.2055	.6165	.8220	1.0405	.79	.75
300	.0289	.1525	.5407	.6932	.7221	.96	.78

For all three cases the values of g and f utilized were 0.75 and 0.5, respectively. The values for 250 nm appear to be optimistic while the values for 300 nm appear to be somewhat pessimistic.

C. DESCRIPTION OF THE CHARACTERISTICS OF THE SIMULATION

The purpose of this simulation was to provide approximate results for the multiple scattering problem. By assuming various source, propagation, and detector characteristics, a user could in principle predict the effectiveness of a proposed system.

The Monte Carlo method described in Appendix A was employed to generate information detailing characteristic patterns of photon scattering as a function of wavelength, position of an observer, pulse spreading, and field of view of the detector being employed. The observer may be located at any arbitrary angle off from the axis of propagation and at any arbitrary distance from the source (measured in extinction lengths).

Of primary interest were the characteristic patterns of multiply scattered radiation. The simulation provided for obtaining diagrams of photon flux at a given position as viewed by either the source or the receiver. In addition, the patterns received by the detector were capable of being limited by field of view restrictions. By measuring the photon flux at a given position, contours of equal photon flux were generated. These contours provided a simple means of visualizing the radiation patterns.

Detector field of view considerations indicate the field of view required to receive a given threshold of photons at a fixed position as well as the maximum range at a given angle that a threshold number of photons can be

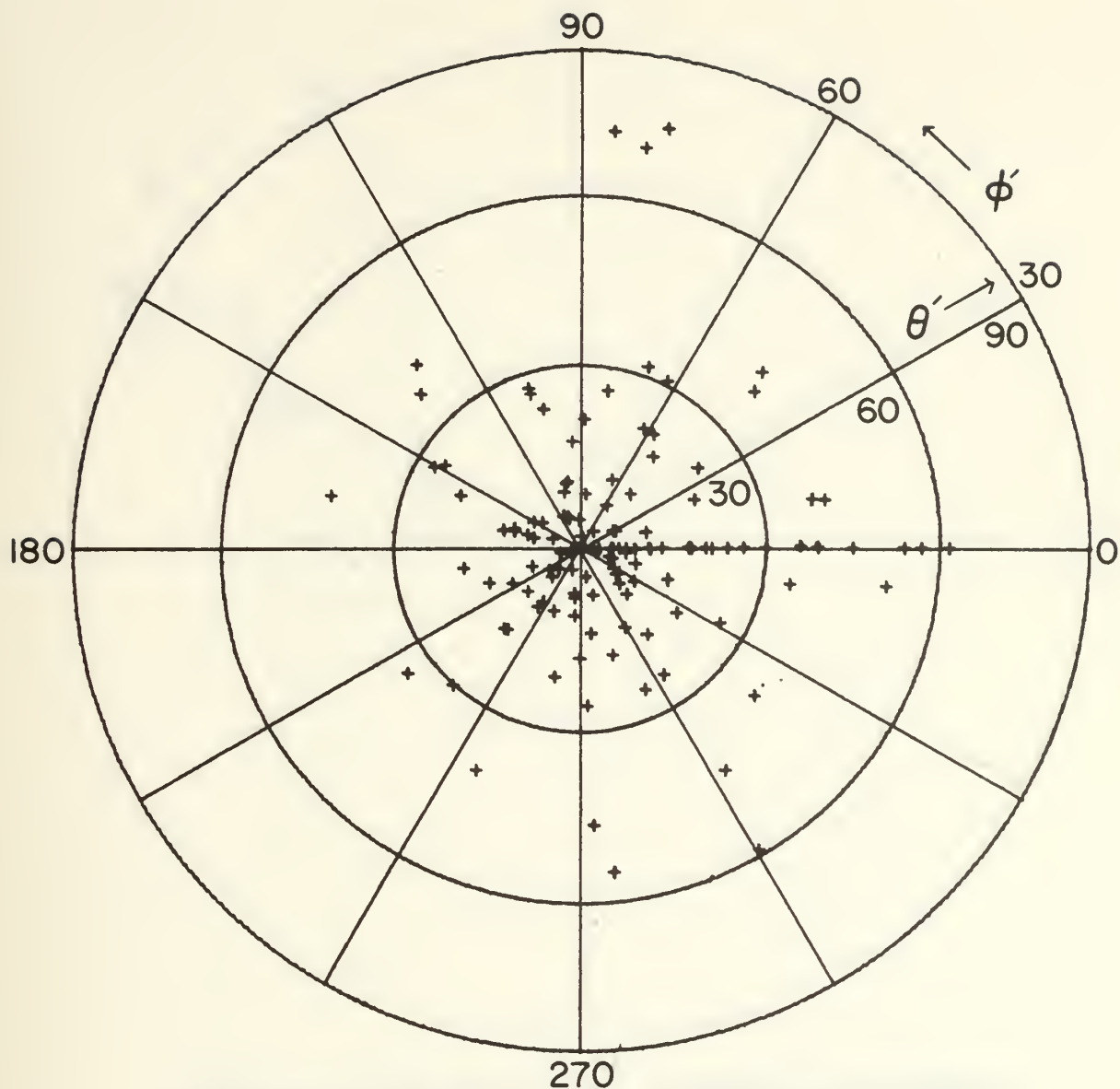
detected for a fixed field of view. Finally, pulse spreading information due to the time delay caused by multiple scattering was also available.

D. CHARACTERISTIC PATTERNS OF MULTIPLY SCATTERED RADIATION

Figures 4 and 5 represent the pattern of photons received by a 180 degree field of view detector located zero to nine and 36 to 45 degrees off from the axis of propagation respectively at one extinction length from a 300 nm laser source. As the detector approached the axis of propagation more photons were received. The photons along the ϕ prime equal to zero axis represent single scattered radiation. Many of the photons received were, however, multiply scattered.

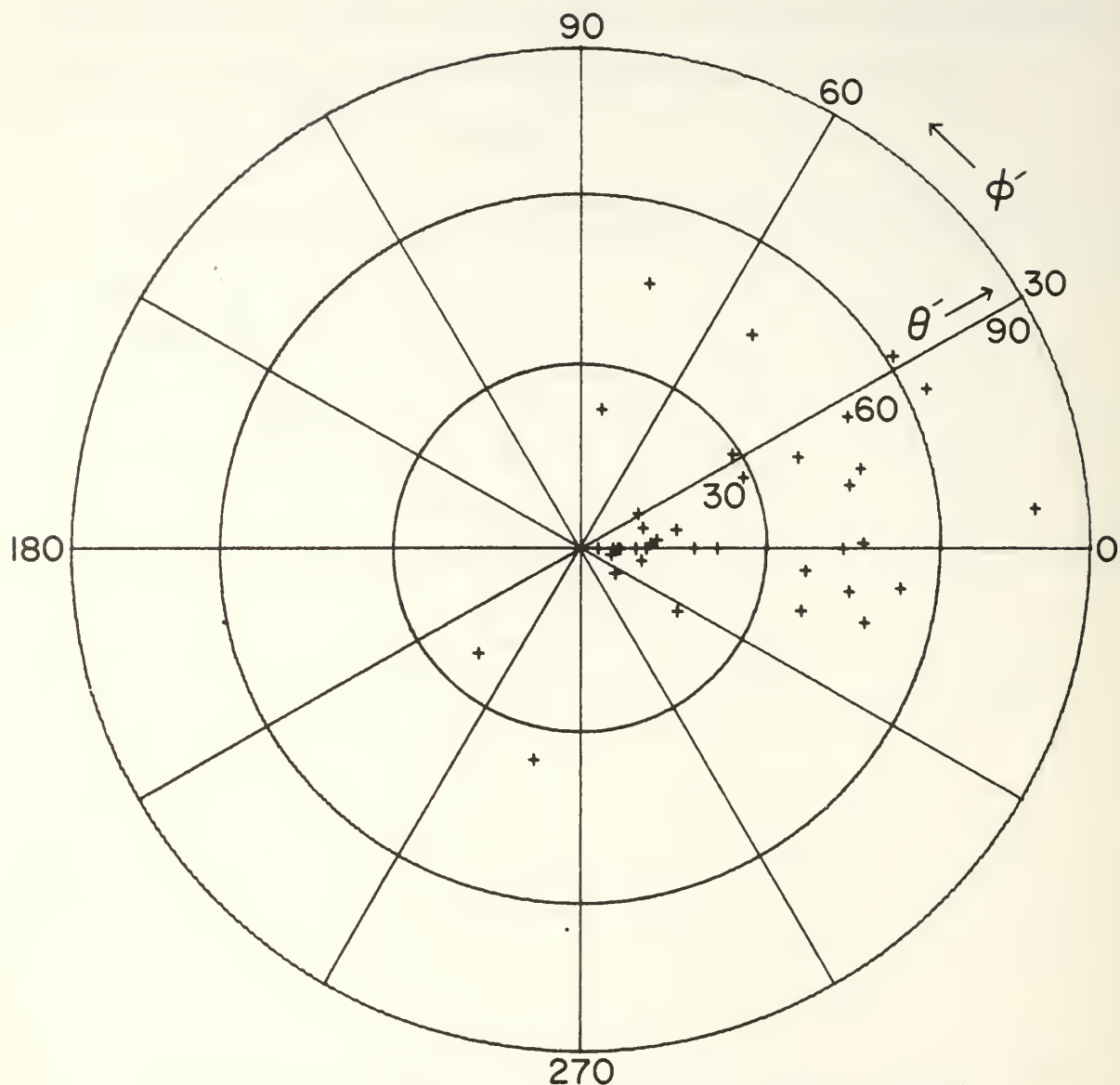
Figures 4 and 5 are similar to Figures 6 and 7 only in the latter figures the receiver is located five extinction lengths from the source. The percentages of multiply scattered photons increases greatly as the receiver is moved either off from the axis of propagation or away from the source. At five extinction lengths, virtually none of the radiation received is single scattered. This is a strong indication of the hazards of single scattering models in the middle uv.

Figures 8, 9, and 10 represent the contours of equal photon flux for 250, 280, and 300 nm wavelengths. The label for each contour is



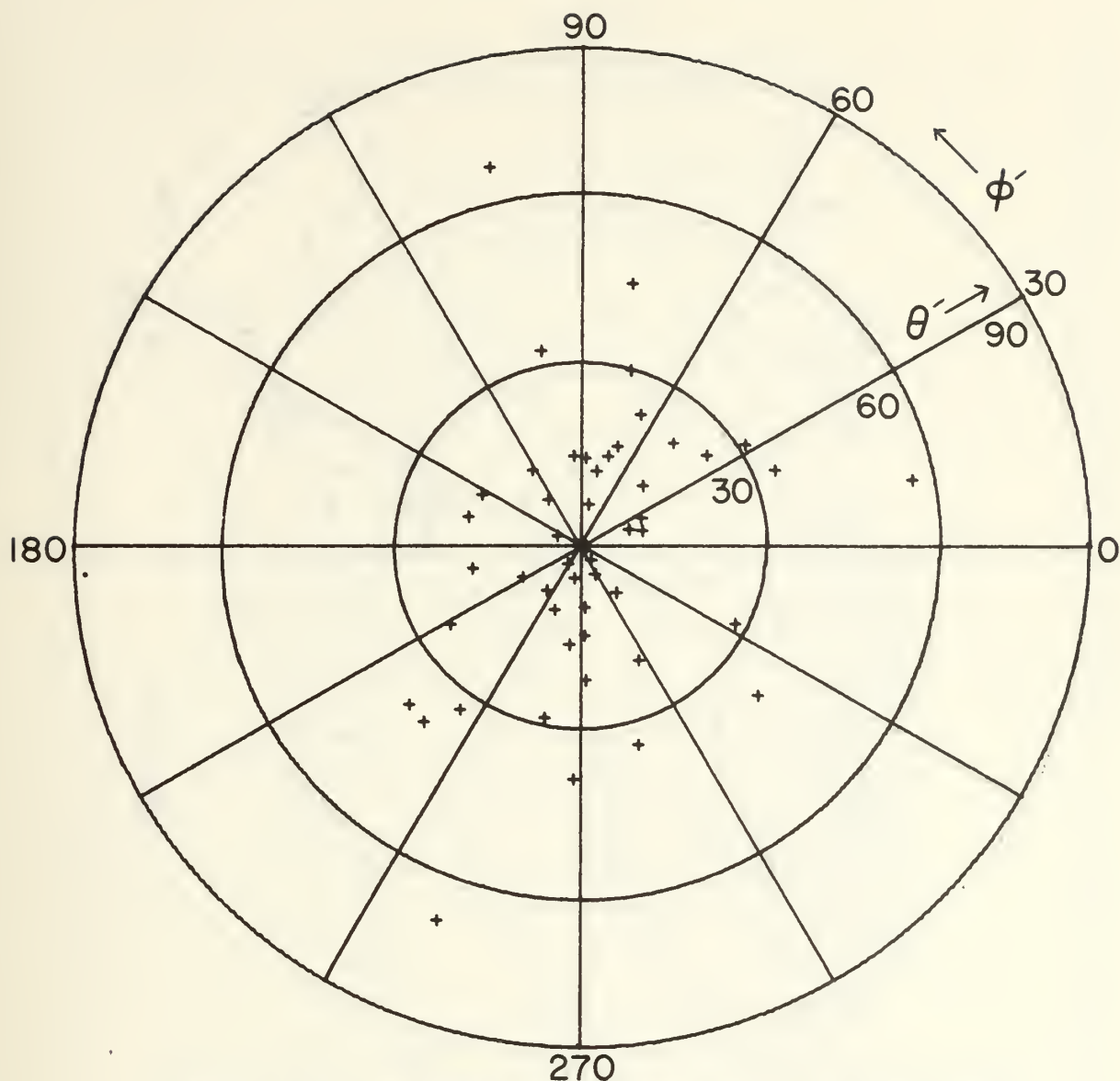
270
 RECEIVER LOCATED ONE EXTINCTION LENGTH
 FROM THE SOURCE. $\theta = 0$ TO 9 DEGREES
 $\lambda = 300$ NM. FIELD OF VIEW = 180 DEGREES

FIGURE 4. Photon Scattering Diagram (θ' vs ϕ') as Viewed by a Receiver Located θ Degrees from the Axis of Propagation.



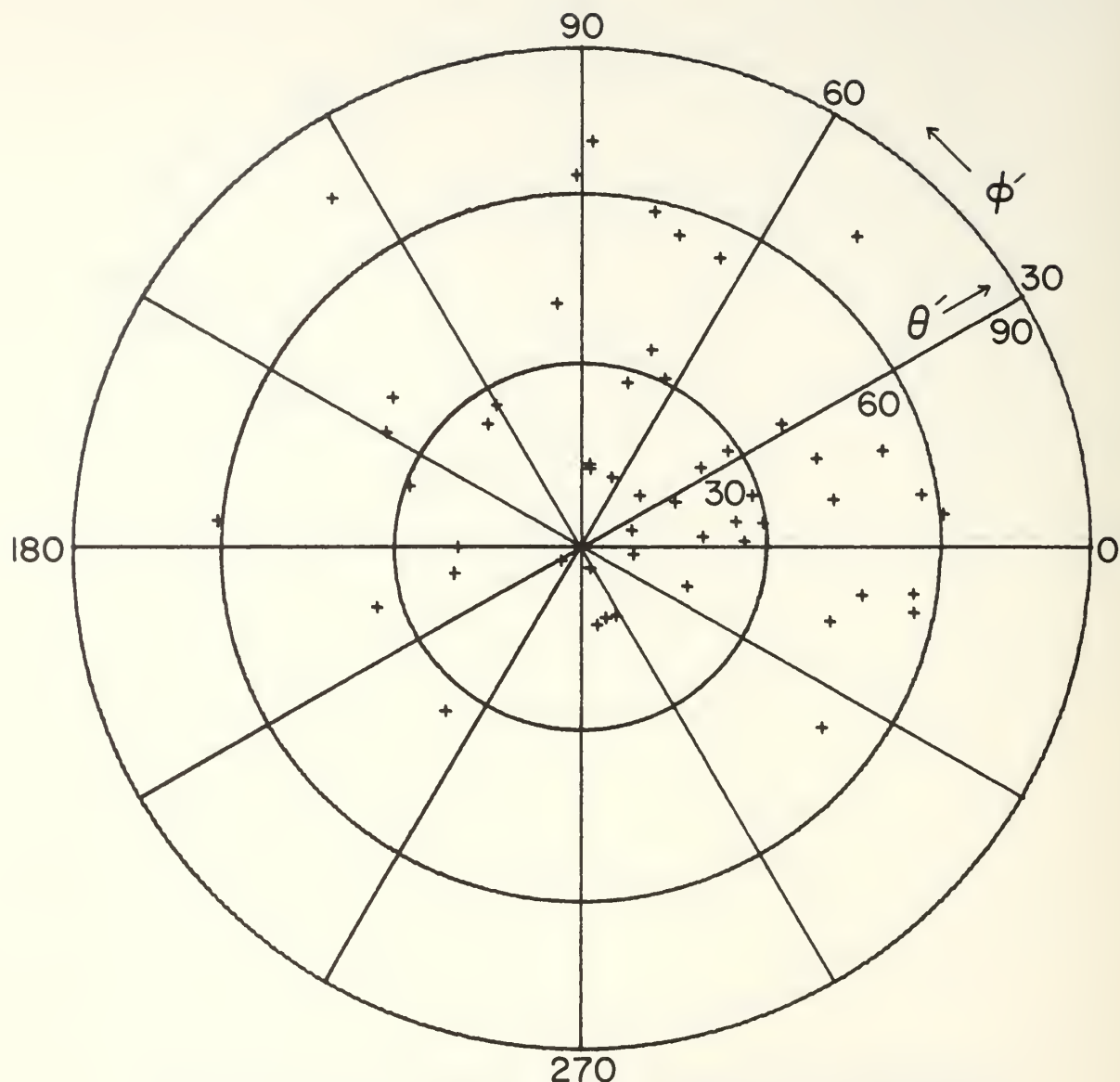
RECEIVER LOCATED ONE EXTINCTION LENGTH
FROM THE SOURCE. $\theta = 36$ TO 45 DEGREES
 $\lambda = 300$ NM. FIELD OF VIEW = 180 DEGREES

FIGURE 5. Photon Scattering Diagram (θ' vs ϕ') as Viewed by a Receiver Located θ Degrees from the Axis of Propagation.



RECEIVER LOCATED FIVE EXTINCTION LENGTHS
FROM THE SOURCE. $\theta = 0$ TO 9 DEGREES
 $\lambda = 300$ NM. FIELD OF VIEW = 180 DEGREES

FIGURE 6. Photon Scattering Diagram (θ' vs ϕ') as Viewed by a Receiver Located θ Degrees from the Axis of Propagation



RECEIVER LOCATED FIVE EXTINCTION LENGTHS
FROM THE SOURCE. $\theta = 36$ TO 45 DEGREES
 $\lambda = 300$ NM. FIELD OF VIEW = 180 DEGREES

FIGURE 7. Photon Scattering Diagram (θ' vs ϕ') as Viewed by a Receiver Located θ Degrees from the Axis of Propagation

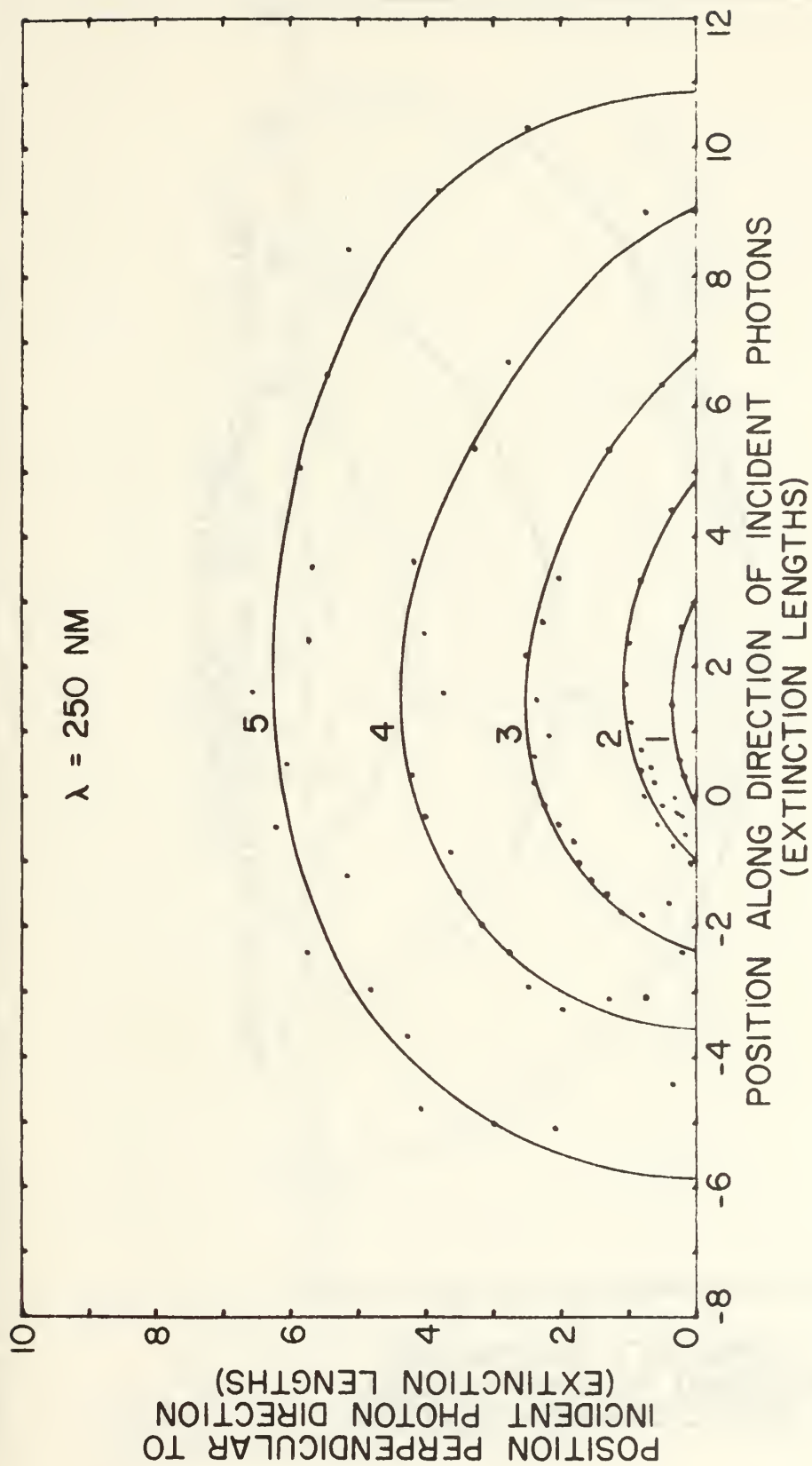


FIGURE 8. Contours of Equal Photon Flux as a Function of the Position of the Observer

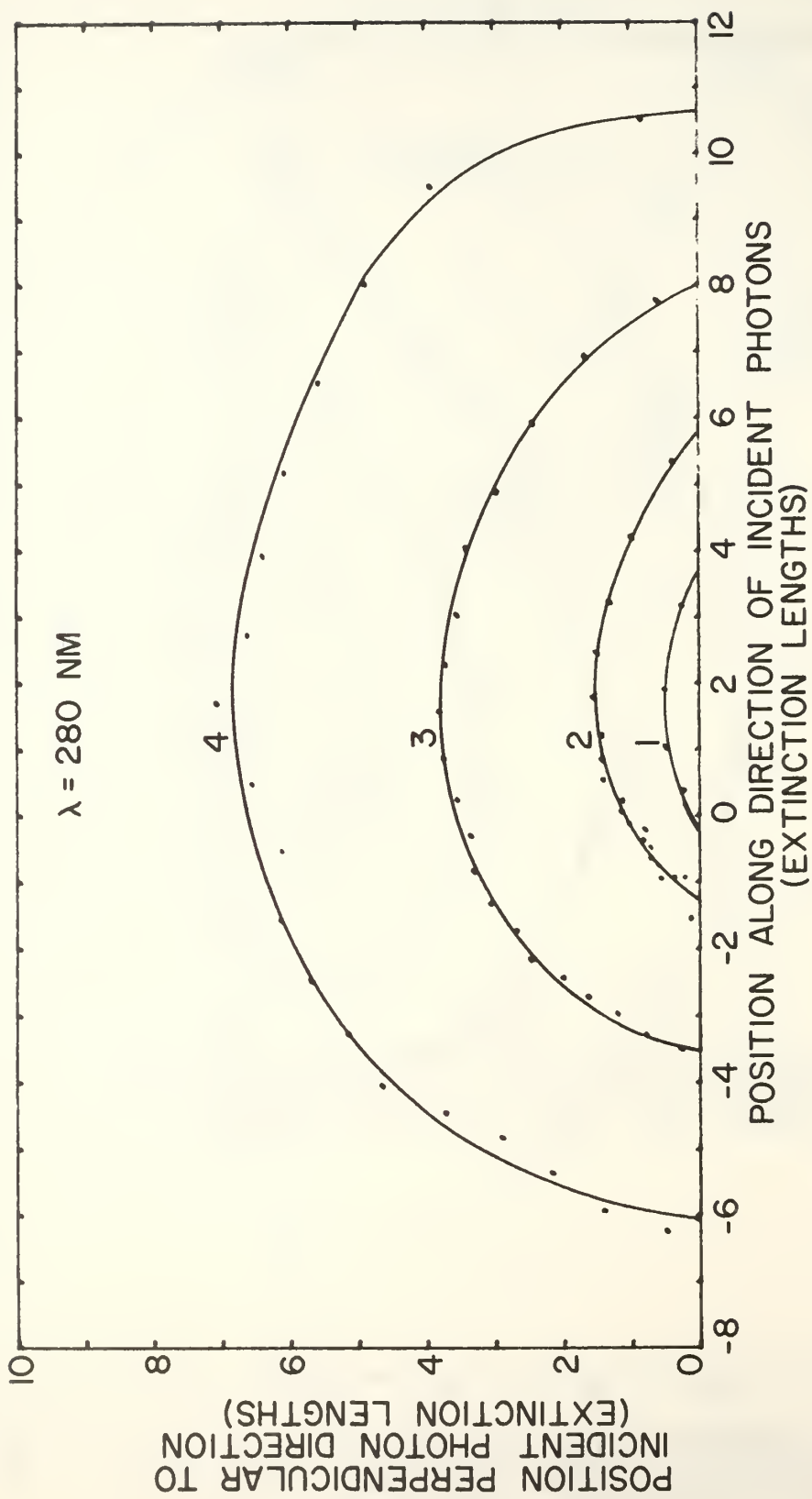


FIGURE 9. Contours of Equal Photon Flux as a Function of the Position of the Observer

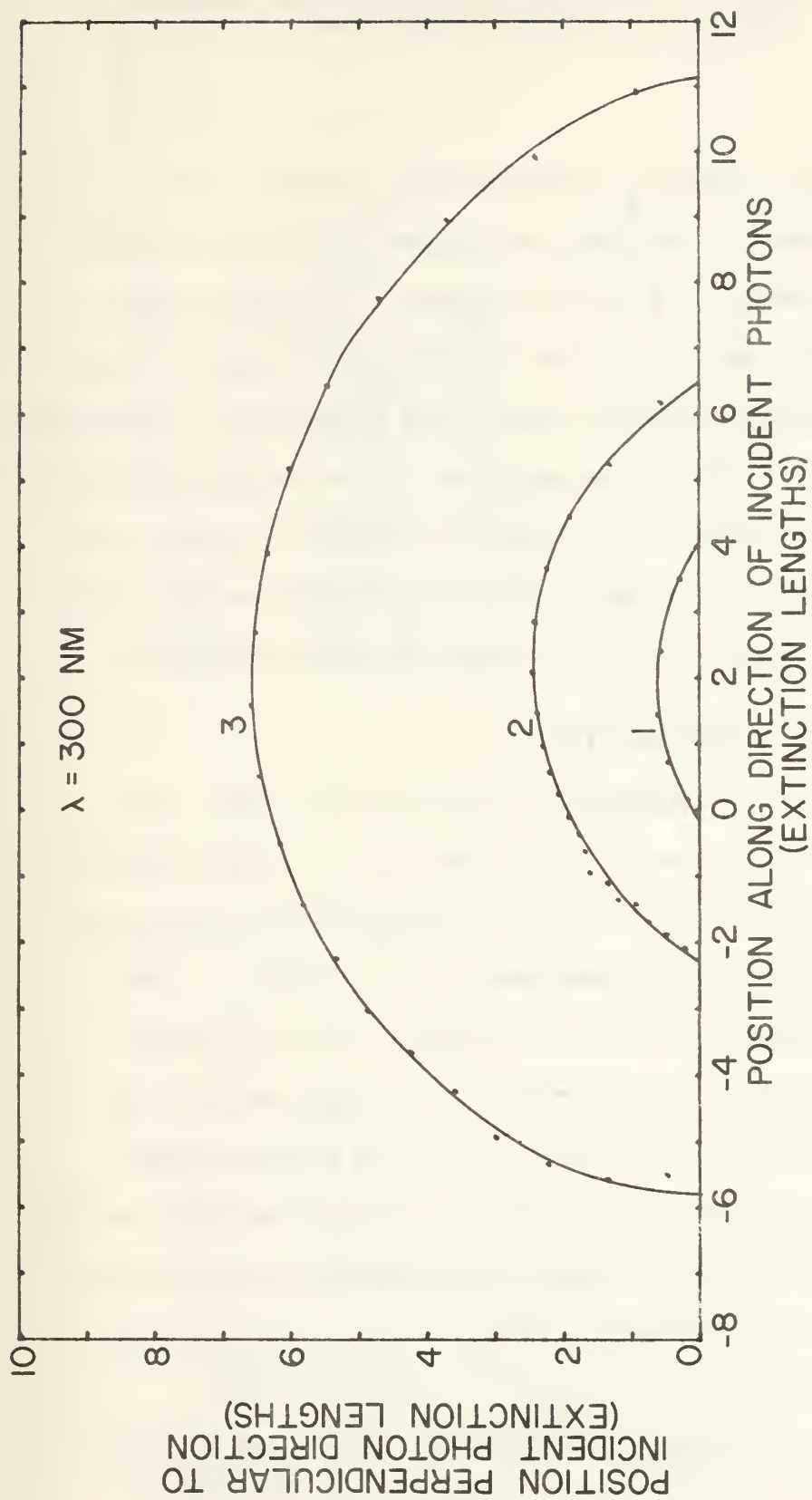


FIGURE 10. Contours of Equal Photon Flux as a Function of the Position of the Observer

$$\text{Relative Flux} = -\log_{10} \left[\frac{N}{N_0 2\pi R^2 (\cos\theta_1 - \cos\theta_2)} \right] \quad (4)$$

where $2\pi R^2 (\cos\theta_1 - \cos\theta_2)$ is the area of that portion of a hemisphere located R extinction lengths from the source subtended by θ_1 and θ_2 , N is the number of photons penetrating that area, and N_0 is the number of photons leaving the source. Each successive contour of photon flux represents a decrease of one order of magnitude in the relative photon flux. Thus, for example, the contour labeled 2 gives the location at which the photon flux is 10^{-2} photons per unit area, where unit area is one extinction length squared.

E. FIELD OF VIEW CONSIDERATIONS

Figures 11 and 12 represent the relative number of photons detected at a receiver located zero to nine and 36 to 45 degrees off from the axis of propagation at one and five extinction lengths respectively from a 250 nm laser source. A sixty degree (full cone angle) field of view detector would receive seventy-five to eighty percent of the incident radiation for the θ_1 (zero to nine degrees) and the θ_2 (36 to 45 degrees) cases at one extinction length. At five extinction lengths these percentages tend to remain stable. Thus, given a minimum required photon flux at a detector, it is possible to select the proper field of view for that detector. Conversely, utilizing a fixed

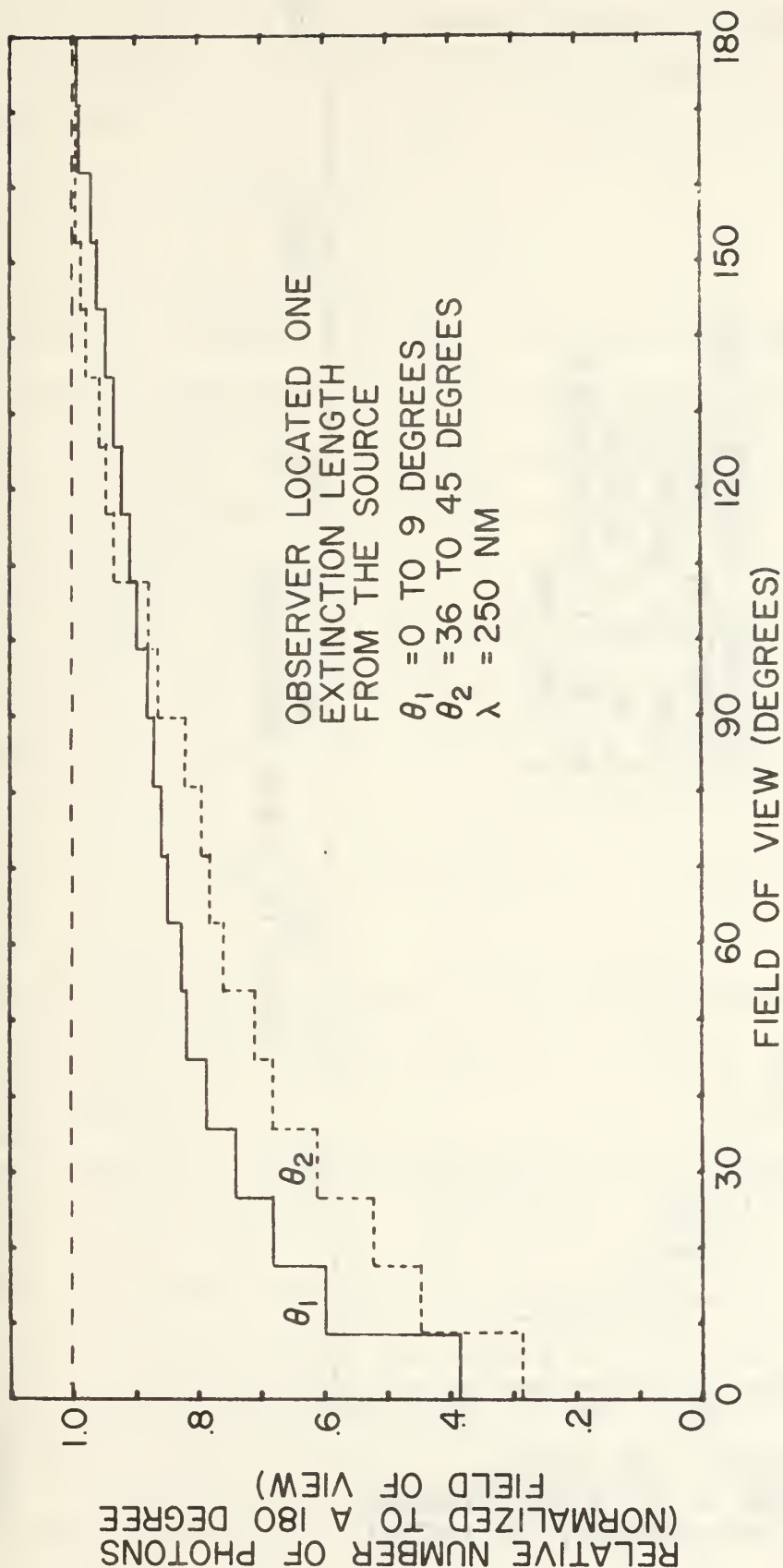


FIGURE 11. Relative Number of Photons vs Field of View for an Observer Located θ Degrees from the Axis of Propagation

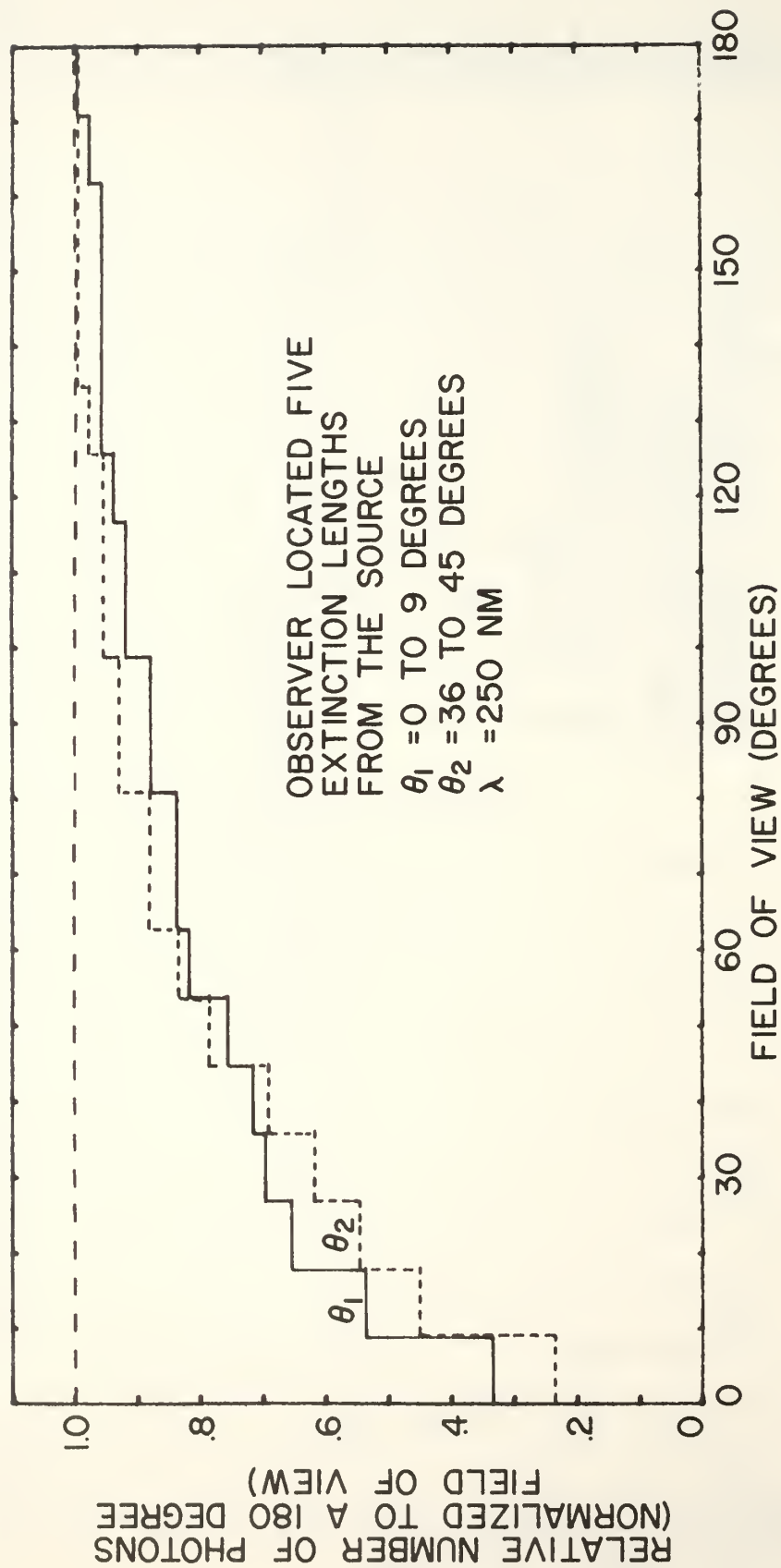


FIGURE 12. Relative Number of Photons vs Field of View for an Observer Located θ Degrees from the Axis of Propagation

field of view detector, it is possible to determine the maximum effective range for a minimum photon flux. (The results for 280 and 300 nm were substantially the same as the 250 nm simulation).

F. PULSE SPREADING CONSIDERATIONS

Figures 13 and 14 represent the pulse spreading as received by a detector located zero to nine and 36 to 45 degrees off from the axis of propagation at one and five extinction lengths from a 250 nm laser source, respectively. The pulse spreading function is a function of the position of the observer and time dispersion caused by multiple scattering. The relative time dispersion, $T(R,D)$ is defined as follows:

$$T(R,D) = \frac{D}{R} - 1 \quad (5)$$

where D is the total distance traveled by each photon and R is the distance from the source to the shell penetrated by each photon.

The results of pulse spreading at other distances and angles was examined. The pulse spreading function is nearly constant for values of R from one to ten extinction lengths, thus one figure suffices as an approximation to any distance in this angular range. The increase in pulse spreading with increasing angle is illustrated with one additional plot at 36 to 45 degrees off from the

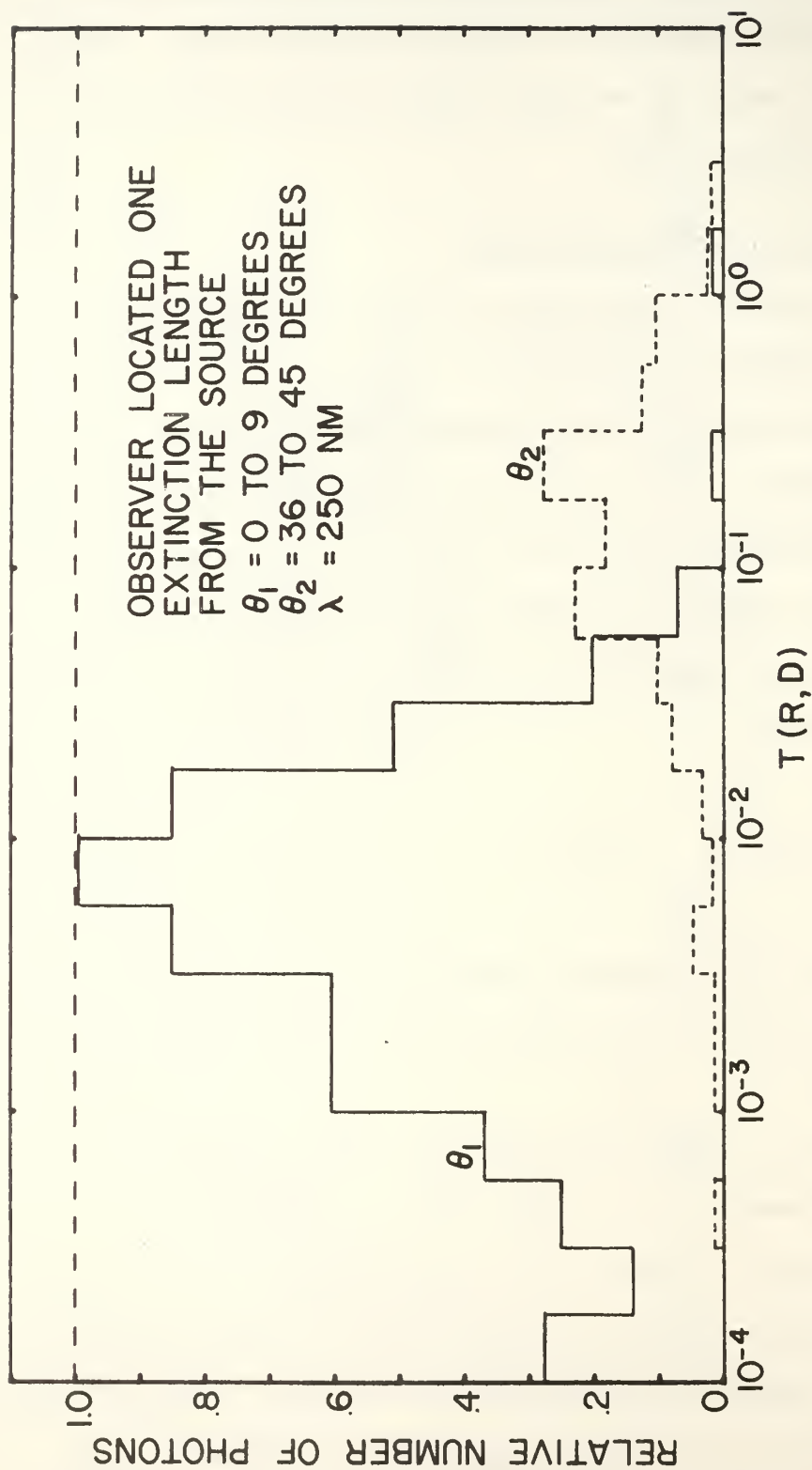


FIGURE 13. Pulse Spreading for an Observer Located θ Degrees from the Axis of Propagation

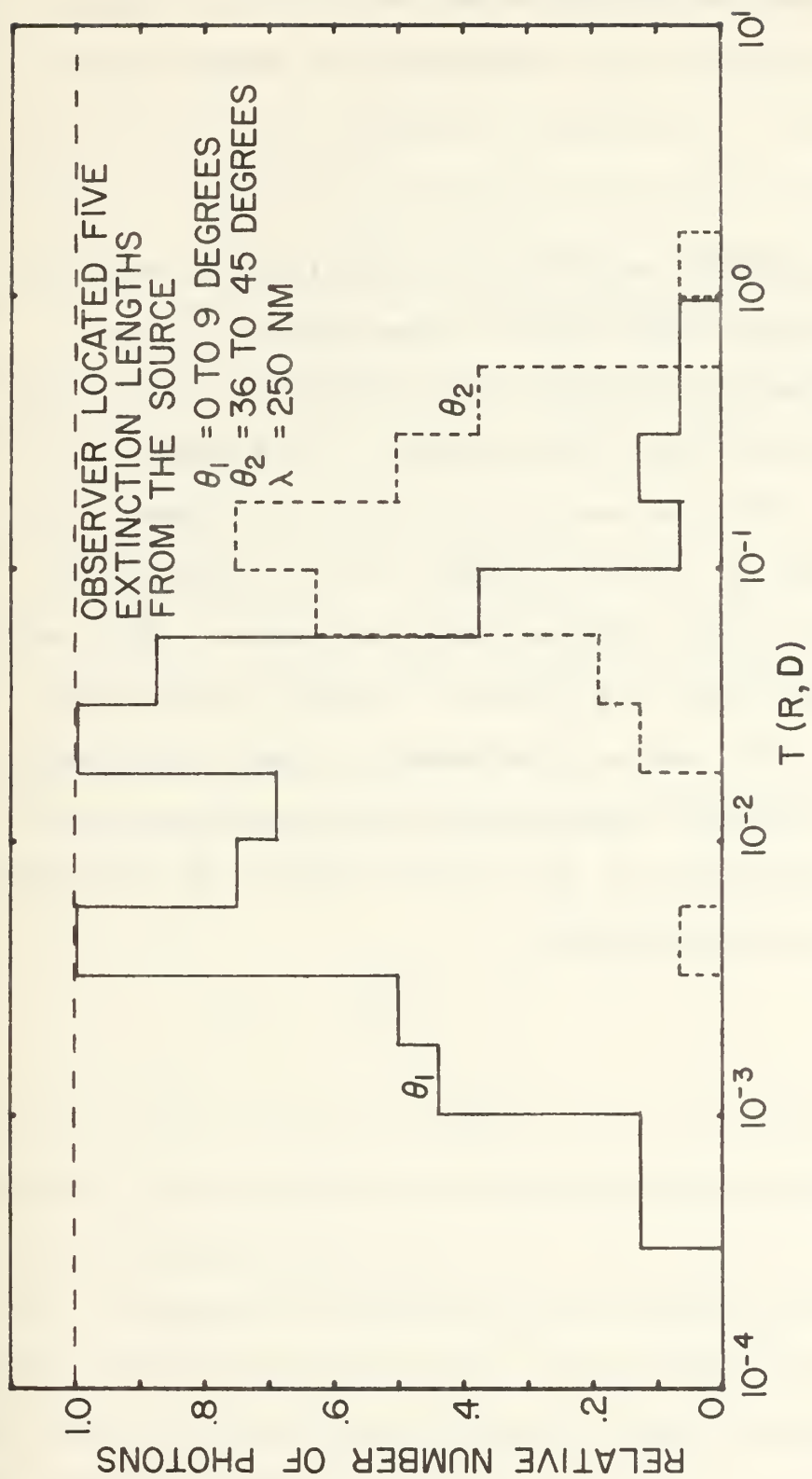


FIGURE 14. Pulse Spreading for an Observer Located Degrees from the Axis of Propagation

axis of propagation. Reproduction of the results at each cone angle introduces a cumbersome presentation of this information, hence only one representative sample is included.

G. SUMMARY

The absorption and scattering coefficients as well as the phase functions from previous experiments were utilized and the behavior of multiple scattered radiation was simulated using the Monte Carlo method. This model was used to study the characteristics of the source beam at a receiver located an arbitrary angle off from the axis of propagation at a given distance from the source. With such information available, the geometric pattern of possible communication links can be determined. A photon density as a function of receiver field of view and position of the observer was determined as well as the effects of multiple scattering on pulse spreading.

VI. SIGNAL-TO-NOISE CONSIDERATIONS

A. INTRODUCTION

The photon flux information presented in the previous section may be utilized to estimate the signal-to-noise ratio (S/N or SNR). This information, however, must be used in conjunction with the characteristics of the detector. Additional considerations therefore include the characteristics of the optical filter, quantum efficiency of the detector, background level of radiation, etc. This section considers the characteristics of available devices and of known atmospheric flux levels in order to estimate the flux level necessary for reliable communication.

B. FUNDAMENTAL RELATIONSHIPS

The detector current generated by a light signal of power P_S and of frequency ν is

$$i_S = \frac{G\eta e P_S}{h\nu} \quad (6)$$

where G is the gain of the detector, η is the quantum efficiency of the detector, e is the electronic charge, and h is Planck's constant [18].

The dominant noise mechanism for detectors operating in the visible and ultraviolet region of the spectrum is shot noise. The mean square of the noise current due to this noise mechanism is

$$\langle i_n^2 \rangle = 2eG^2 \left[i_d + \frac{\eta e}{h\nu} (P_S + P_B) \right] B \quad (7)$$

where G is the gain of the detection device (typically a photomultiplier), i_d is the dark current, P_B is the power of the background radiation present due to sources other than that from the desired signal, and B is the bandwidth of the receiver [18, 25, 26, 27].

The desired expression for S/N is thus the ratio of the square of Equations (6) and of (7).

$$S/N = \frac{\langle i_s^2 \rangle}{\langle i_n^2 \rangle} = \frac{\left(\frac{\eta P_S}{h\nu} \right)^2}{2e \left[i_d + \frac{\eta e}{h\nu} (P_S + P_B) \right] B} \quad (8)$$

In several specific cases the dark current i_d is negligible, whereupon Equation (8) reduces to Equation (9).

$$S/N \approx \frac{\eta P_S}{2h\nu B} \left(\frac{P_S}{P_S + P_B} \right) \quad (9)$$

For pulsed signals having a time duration of τ , the bandwidth B is effectively $1/2\tau$. The relationship for S/N thus reduces to the number of photons converted to electrons in a pulse, degraded by the ratio of the signal power to total power received over the duration of the pulse.

Each of the expressions for S/N may be modified slightly by consideration of a duty factor, introduced to account for the fact that a signal is not constant over the duration

of a pulse. Consideration of this introduces a multiplicative factor equal to Equation (10).

$$\frac{D_S}{D_N} = \frac{\int_{-\tau/2}^{\tau/2} \left(\frac{i_S(t)}{i_S(0)} \right)^2 dt}{\int_{-\tau/2}^{\tau/2} \left(\frac{i_N(t)}{i_N(0)} \right)^2 dt} \quad (10)$$

where D_S/D_N is the ratio of the duty factor of the signal to that of the noise over the duration of the pulse, τ .

C. BACKGROUND LEVELS OF RADIATION

The expressions for S/N involve critically the background levels of radiation due to other sources. In communication experiments this is typically due to scattered sunlight. Reliable flux levels at wavelengths longer than 300 nm are reported by Valley [28]. The flux levels at shorter wavelengths are a result of both direct and diffuse transmission. These levels are critically dependent on the thickness of the ozone layer, and have been calculated for various atmospheric conditions [12].

The photon flux calculated by Shettle and Green is presented in Table IV. The dramatic drop in background radiation levels at around 280 nm is evident. The signal that would be transmitted through a narrow band (10 nm) multilayer dielectric filter at 300 nm would include up to 10^{13} photons/cm² as background noise photons, whereas at

wavelengths below 280 nm this background radiation level may be considered to be quite small.

TABLE IV

Photon Flux Due to Direct and Diffuse
Transmittance through the Earth's
Atmosphere [12]

A solar angle of ninety degrees is assumed, along with a 0.32 cm ozone thickness.

λ (nm)	Flux (watts/m ² nm)	Flux (photons/cm ² nm sec)
300	1.07×10^{-2}	1.6×10^{12}
295	5.15×10^{-4}	7.8×10^{10}
290	2.14×10^{-6}	3.2×10^8
285	9.50×10^{-11}	1.4×10^4
280	9.09×10^{-19}	1.4×10^{-4}

D. DETECTOR CHARACTERISTICS

The detector characteristics which relate to a given S/N expression include filter characteristics, quantum efficiency, detector area, and field of view. Using a combination of multilayer dielectric filters and absorption filters, it is possible to construct a device having composite characteristics which will pass ten percent of the incident flux at 265 nm and reject the ambient solar flux in the visible to a degree sufficient to reduce the overall background count level to approximately ten counts per

second [29]. The transmission characteristics of this filter in the 200 to 400 nm region are indicated in Figure 15. It is thus expected that somewhat greater than one percent but less than ten percent of the photons in the 250 to 280 nm region will pass through the filter. Once the photons reach the photocathode of a typical photomultiplier, the conversion efficiency is usually greater than ten percent but less than 25 percent. Thus, for purposes of estimating S/N, the combined effects of filter transmission characteristics plus quantum efficiency of the photocathode may be accounted for by choosing a value of η to be greater than 10^{-3} but less than 10^{-2} . With unforeseen developments it is possible to expect a combination having a composite value of 10^{-1} , however such a device is not presently available.

The area of the detector used in the simulation was chosen to be nominally one square inch, typical of currently available photomultiplier tubes.

E. STATISTICAL CONSIDERATIONS

The number of photons converted into an electrical signal follows Poisson statistics:

$$P(r) = e^{-n} n^r / r! \quad (11)$$

where $P(r)$ is the probability that r photons are observed in a sample pulse which has an average number of n photons per pulse.

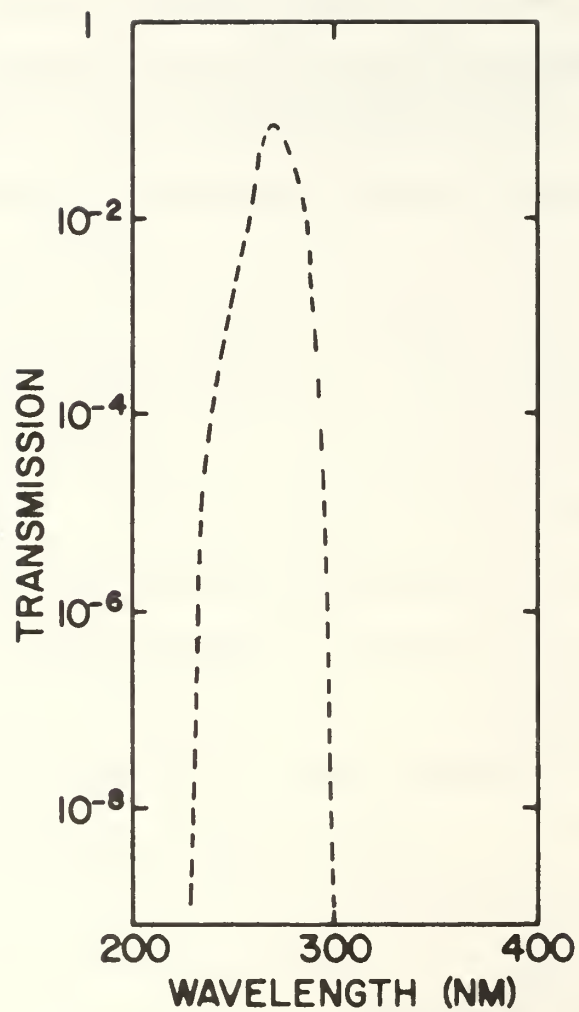


FIGURE 15. Transmission Characteristics for a Typical Composite Filter

The probability of observing an event with a number of photons above the threshold value r_{th} is

$$P(r > r_{th}) = \sum_{r=r_{th}}^{\infty} \frac{e^{-n} n^r}{r!} \quad (12)$$

Graphs of this function are readily available [30]. Given an average number, n , equal to ten and a threshold level of two (to distinguish from the random single photon events which occur at the detector with a frequency of occurrence equal to ten or twenty photons per second), a probability of detection of such pulses is .9995. If the average number n is five with the threshold number equal to two, the probability of detection is 0.96. Thus an average value of ten photons per pulse in the absence of background radiation is chosen as a desired level to avoid excessive error. This means that a desirable value of S/N is ten.

F. SUMMARY OF SIGNAL-TO-NOISE CONSIDERATIONS

For the case of minimal background radiation, Eq. (13) gives the relationship for the number of signal photons required.

$$\frac{P_s \tau}{h\nu} = \frac{1}{\eta} \left(\frac{S}{N} \right) \quad (13)$$

If background radiation dominates the power incident on the detector (as would be the case at wavelengths longer than 300 nm), then the number of signal photons required is given by Eq. (14).

$$\frac{P_S \tau}{h\nu} = \left[\frac{1}{\eta} \left(\frac{S}{N} \right) \left(\frac{P_B \tau}{h\nu} \right) \right]^{1/2} \quad (14)$$

Table V gives a summary of the necessary photon flux external to the detector in order to obtain a S/N equal to ten. These flux levels may be used in conjunction with the figures of Section V to generate the geometric patterns over which signal transmission may be expected.

TABLE V

Photon Flux Required in order to Give
a S/N Equal to Ten

Assumed parameters:

Filter characteristics for Figure 15

Quantum efficiency of ten percent

$\tau = 10^{-6}$ seconds (significant pulse spreading)

Area of detector is one square inch

Note: Filter characteristics at 300 nm have been assumed for a narrow band (ten nm) multilayer dielectric filter.

λ (nm)	η	$\frac{P_B}{h\nu}$ (photons/sec)	$\frac{P_S \tau}{h\nu}$ (photons)	Required flux (photons/cm ²)
250	10^{-3}	---	10^4	1.6×10^3
265	10^{-2}	---	10^3	1.6×10^2
280	10^{-3}	---	10^4	1.6×10^3
300	10^{-2}	10^{13}	10^5	1.6×10^4

VII. DISCUSSION

Although not currently available, three millijoule laser sources of different wavelengths (250, 280, and 300 nanometers) capable of being pulsed at an appropriate rate (200 pulses per second for 2400 bit per second data rate using 12 bits per pulse [4]) were assumed. (The navy has used vocoders with 2400 bits per second capability since the 1940's). Table V lists the assumptions leading to the required photon flux in order to achieve a S/N equal to ten. By utilizing the contours of equal photon flux in Figures 8, 9, and 10, the ranges for which pulse position modulation communication is possible were predicted. Table VI lists the results of these calculations.

Predicted performance for lasers operating at 250 and 280 nm are comparable for sixty degree or greater off axis detection. For detection angles less than sixty degrees the 280 nm laser is superior. The performance of the 300 nm laser does not appear to be degraded by the background radiation as much as might be expected. The performance for this laser from zero to twenty degrees off from the axis of propagation is similar to the 280 nm laser. Beyond thirty degrees the ranges decrease markedly, indicating very little backscattering. It cannot be overstressed that the results above are for a simulation of assumed laser sources with assumed atmospheric propagation

TABLE VI

Predicted Ranges or Range Bands for Communication
in the Middle UV for Pulsed Millijoule Lasers

(θ is the angular location of the receiver
with respect to the axis of propagation.)

$\lambda = 250\text{nm}$ $(1.6 \times 10^3 \frac{\text{Photons}}{\text{cm}^2} \text{ req'd})$		$\lambda = 280\text{nm}$ $(1.6 \times 10^3 \frac{\text{Photons}}{\text{cm}^2} \text{ req'd})$		$\lambda = 300\text{nm}$ $(1.6 \times 10^4 \frac{\text{Photons}}{\text{cm}^2} \text{ req'd})$	
θ (Degrees)	Range (km)	θ (Degrees)	Range (km)	θ (Degrees)	Range (km)
0	2.4	0	5.5	0	5.2
30	1.1	30	2.9	10	3.6
60	.52	60	1.6	20	2.2
90	.34	90	1.0	30	.93
120	.30	120	.92	40	.24
150	.33	150	.94	90	.10
180	.49	180	1.2	180	.10

(Ranges for $\lambda = 250$ nm should be approximately half-way between the ranges listed.)

(Ranges for $\lambda = 280$ nm should be on the order of the range listed.)

(Ranges for $\lambda = 300$ nm should be somewhat less than the range listed.)

characteristics and assumed detector characteristics. Clearly, in order to make accurate predictions for real systems it is necessary to obtain accurate atmospheric characteristics as well as other system parameters.

VIII. CONCLUSION

Lasers operating in the middle uv do not appear to be suitable for long range communications; however, they present definite possibilities for short range (several km) applications. Since radiation in this region is absorbed exponentially, rather than as the inverse of distance squared, the potential for covertness is highly accentuated. Current lasers, however, having a power output on the order of 0.1 joules or greater with low pulse rates (15 to 20 pulses per second), are not suitable for voice communication due to the low repetition rates. The pulsed mode of operation appears to hold definite advantages over amplitude modulation of a continuous wave laser from simple signal-to-noise considerations. Good possibilities for successful communication are offered by pulse position modulation. Millijoule laser sources operating with 200 or more pulses per second are desirable but not currently available.

The contours of equal photon flux presented in this paper are useful for determining the communication patterns of possible laser sources. The pulse spreading and field of view figures are likewise useful for predicting the characteristics of proposed receivers. A multiple scattering model is definitely required for proper prediction of photon flux over expected distances of communication.

APPENDIX A

MONTE CARLO SIMULATION OF THE MULTIPLE SCATTERING PROBLEM

A. FUNDAMENTAL RELATIONSHIPS

1. Weighting Factors for Monte Carlo Calculations

The following calculations served as a model for the derivation of the various weighting factors:

PROBLEM: Given a random number generator that provides numbers within a specified interval along the x-axis (with equal probability for each interval dx) obtain random numbers with a probability $p(y)$. I.e., Find $y(x)$ such that $p(y)dy = dx$.

SOLUTION: Let Random Variable Y be distributed in $y_0 \leq y \leq y_2$ and its density function be given by

$$p(y) = \begin{cases} p(y) & y_0 \leq y \leq y_2 \\ 0 & \text{otherwise} \end{cases}.$$

The distribution function, $P(y)$, is given by

$$P(y) = P(Y \leq y) = \int_{-\infty}^y p(y) dy$$

$$\text{Therefore, } P(y) = \int_{y_0}^y p(y) dy, \text{ since } p(y) = 0 \text{ for } y < y_0.$$

Now,

$$p(y) dy = dx$$

Integrating,

$$y(x) = y_0 + P^{-1}(\Delta x)$$

where

$$y_0 = y(x_0)$$

and $\Delta x = x - x_0$

This concept applied to specific cases yields the following fundamental relationships for weighting factors:

a. Exponential

$$p(y) = \frac{1}{\tau} e^{-y/\tau} \quad (0 \leq y \leq \infty)$$

$$y(x) = -\tau \ln(1 - \Delta x)$$

b. Henyey-Greenstein

$$p(\theta) = \frac{(1-g^2)}{2(1+g^2-2g \cos \theta)^{3/2}} \quad (0 \leq \theta \leq \pi)$$

where

$$g = \langle \cos \theta \rangle$$

$$\theta(x) = \cos^{-1} \left\{ \frac{1+g^2}{2g} - \frac{1}{2g} \left[\frac{1-g^2}{2g(\frac{1+g}{2g} - \Delta x)} \right]^2 \right\}$$

c. Modified Henyey-Greenstein [Zachor 1977]

$$p(\theta) = \frac{1-g^2}{2} \left[\frac{1}{(1+g^2-2g \cos \theta)^{3/2}} + \frac{f}{2} \frac{(3 \cos^2 \theta - 1)}{(1+g^2)^{3/2}} \right]$$

$$0 \leq \theta \leq \pi$$

where

$g = \langle \cos \theta \rangle$ and f is a weighting factor.

$$\theta(x) = \cos^{-1} \left\{ \frac{1+g^2}{2g} - \left[\frac{(g^2-1)^2}{8g^3} \right] \frac{1}{[\Delta x - F(\theta) - \frac{1+g}{2g}]^2} \right\}$$

where

$$F(\theta) = \left[\frac{f}{4} \frac{(1-g^2)}{(1+g^2)^{3/2}} \right] (\cos \theta - \cos^3 \theta)$$

d. Uniform

$$p(\phi) = \frac{1}{2\pi} \quad 0 \leq \phi \leq 2\pi$$

$$\phi(x) = 2\pi \Delta x$$

e. Rayleigh

$$p(\theta) = \frac{3}{8}(1 + \cos^2 \theta) \quad 0 \leq \theta \leq \pi$$

$$\theta(x) = \cos^{-1}(A + B)$$

where

$$A = \sqrt[3]{-\frac{b}{2} + \sqrt{\frac{b^2}{4} + 1}}$$

$$B = \sqrt[3]{-\frac{b}{2} - \sqrt{\frac{b^2}{4} + 1}}$$

and

$$b = 8 \Delta x - 4$$

2. Position and Coordinates in Photon-Fixed Coordinate System

a. Axis Rotation

Axis rotation is accomplished by the following transformation:

$$\begin{bmatrix} x' \\ y' \\ z' \end{bmatrix} = \begin{bmatrix} \cos \Delta\theta \cos \Delta\phi & -\cos \Delta\theta \sin \Delta\phi & -\sin \Delta\theta \\ \sin \Delta\phi & \cos \Delta\phi & 0 \\ \sin \Delta\theta \cos \Delta\phi & -\sin \Delta\theta \sin \Delta\phi & \cos \Delta\theta \end{bmatrix} \begin{bmatrix} x \\ y \\ z \end{bmatrix}$$

b. Axis Translation

Axis translation is accomplished by the following transformation:

$$\begin{bmatrix} x'' \\ y'' \\ z'' \end{bmatrix} = \begin{bmatrix} x' \\ y' \\ z' \end{bmatrix} + \Delta r \begin{bmatrix} 0 \\ 0 \\ 1 \end{bmatrix}$$

3. Angles $(\theta, \phi, \theta', \phi')$ for a Photon Passing Through a Shell¹

A laser is located at the origin of the $\hat{i}_0, \hat{j}_0, \hat{k}_0$ coordinate system. The initial direction of propagation of the collimated beam is along the $-\hat{k}_0$ axis. θ is the angle between the position vector \bar{R} (pointing from the location where the photon penetrates a shell toward the laser source) and the vector $-\hat{k}_0$. ϕ is the angle between the projection of $-\bar{R}$ onto the (\hat{i}_0, \hat{j}_0) plane (denoted by $-\bar{R}_p$) and the vector \hat{i}_0 .

A photon is located at the origin of the $\hat{V}_x, \hat{V}_y, \hat{V}_z$ and the $\hat{U}_x, \hat{U}_y, \hat{U}_z$ coordinate systems. As the photon passes through the shell, θ' specifies the angular direction of photon travel (along \hat{U}_z) relative to \bar{R} (the line-of-sight position vector). ϕ' is the angle between the projection of \hat{U}_z (denoted by the vector \bar{W}) onto the (\hat{V}_x, \hat{V}_y) plane and \hat{V}_x .

The vectors \bar{R}_i, \bar{R}_j , and \bar{R}_k are position vectors in the $\hat{U}_x, \hat{U}_y, \hat{U}_z$ coordinate system denoting the location of the points $(1,0,0)$, $(0,1,0)$, and $(0,0,1)$ in the $\hat{i}_0, \hat{j}_0,$

¹See Figure 16.

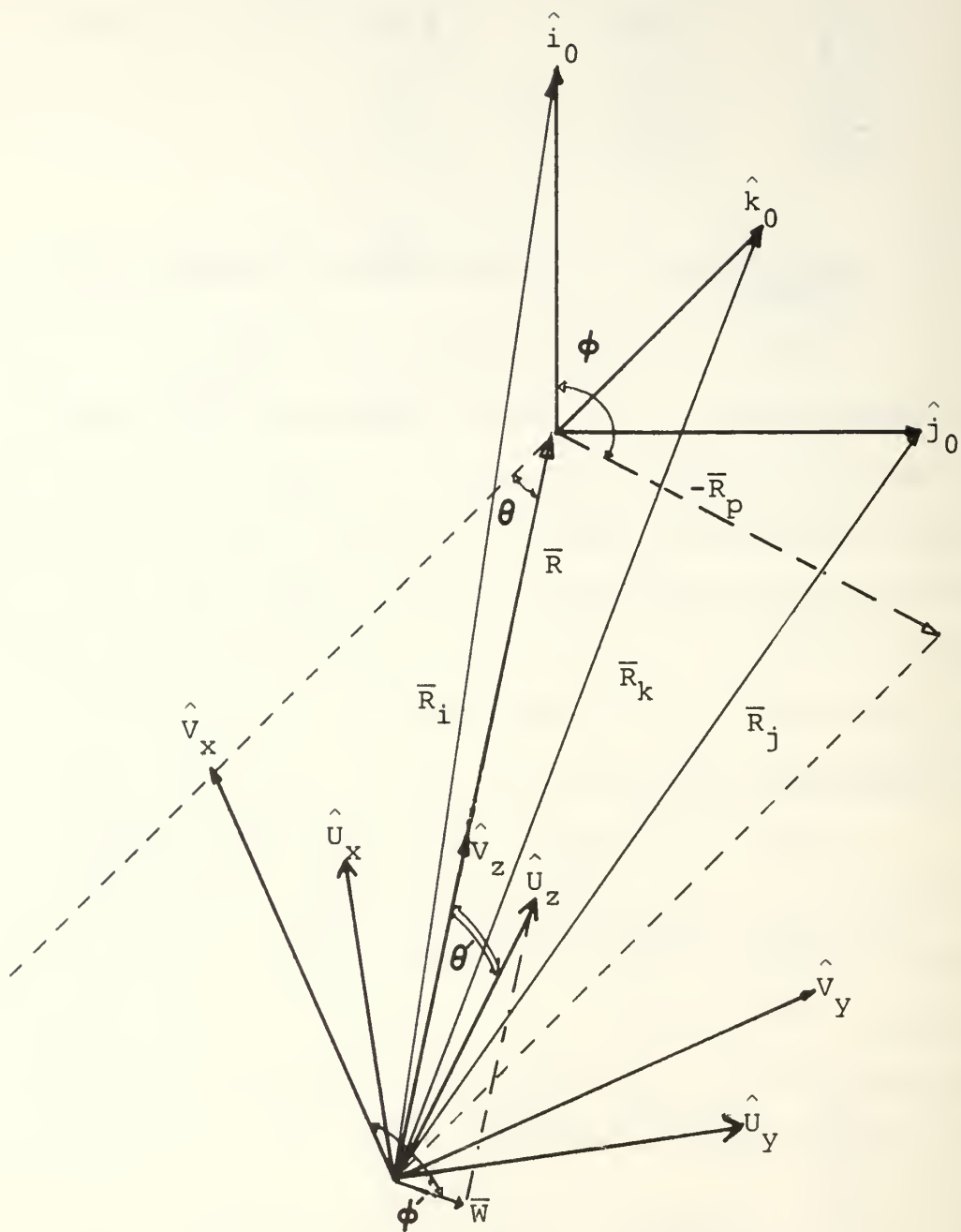


FIGURE 16. Diagram of the Photon Fixed Coordinate System

\hat{k}_o coordinate system. (These points are used for orientation purposes.)

$$\text{a. } \theta = \cos^{-1} \left(\frac{\bar{R} \cdot \hat{k}_o}{|\bar{R}| |\hat{k}_o|} \right)$$

$$\theta = \cos^{-1} \left[\frac{\bar{R} \cdot (\bar{R}_k - \bar{R})}{r} \right] \quad (0 \leq \theta \leq \pi)$$

$$\text{b. } \phi = \cos^{-1} \left(\frac{\bar{R} \cdot \hat{i}_o}{|\bar{R}_p|} \right)$$

$$\phi = \cos^{-1} \left[\frac{\bar{R} \cdot (\bar{R}_i - \bar{R})}{r_p} \right]$$

where

$$r_p = \sqrt{r^2 - [(\bar{R}_K - \bar{R}) \cdot \bar{R}]^2} \quad (0 \leq \phi \leq 2\pi)$$

$$\text{c. } \theta' = \cos^{-1} \left(\frac{\hat{U}_z \cdot \bar{R}}{|\bar{R}|} \right)$$

$$\theta' = \cos^{-1} \left(\frac{\hat{U}_z \cdot \bar{R}}{r} \right) \quad (0 \leq \theta' \leq \pi)$$

$$\text{d. } \phi' = \cos^{-1} \left(\frac{\hat{V}_x \cdot \bar{W}}{w} \right) \quad (0 \leq \phi' \leq 2\pi)$$

where

$$w = 1 - (\hat{V}_z \cdot \hat{U}_z)^2$$

4. Mapping Spherical Coordinates onto Polar Coordinates and Coordinate Transformation

In order to map a point on a sphere onto a circle(s) such that there is a one-to-one mapping the following transformations were utilized:

Case I. $0 \leq \theta \leq \pi/2$

$$r = R \sqrt{1 - \cos \theta}$$

$$\theta = \cos^{-1} \left[1 - \left(\frac{r}{R} \right)^2 \right]$$

Case II. $\pi/2 \leq \theta \leq \pi$

$$r = R \sqrt{1 + \cos \theta}$$

$$\theta = \cos^{-1} \left[\left(\frac{r}{R} \right)^2 - 1 \right]$$

In order to plot (θ, ϕ) the following coordinate transformation was used:

I.e. - Given (θ, ϕ) , find (x, y) .

$$r = \begin{cases} R \sqrt{1 - \cos \theta} & 0 \leq \theta \leq \pi/2 \\ R \sqrt{1 + \cos \theta} & \pi/2 \leq \theta \leq \pi \end{cases}$$

$$x = r \cos \phi$$

$$y = r \sin \phi$$

5. Phase Functions

A factor of $(\frac{1}{2\pi})$ arises from the normalization process for the phase function.

$$\text{(i.e. } \int_0^{2\pi} \int_0^{\pi} p(\theta) \sin \theta d\theta d\phi = 1)$$

a. Particulate

$$P(\theta) = \frac{1-g^2}{4\pi} \left[\frac{1}{(1+g^2-2g \cos \theta)^{3/2}} + \frac{f}{2} \frac{3 \cos^2 \theta - 1}{(1+g^2)^{3/2}} \right]$$

b. Rayleigh

$$P(\theta) = \frac{3}{16\pi} (1 + \cos^2 \theta)$$

APPENDIX B

DEVELOPMENT OF THE FUNDAMENTAL RELATIONSHIP FOR RAYLEIGH SCATTERING

$$p(\theta) = \frac{3}{8} (1 + \cos^2 \theta) \quad 0 \leq \theta \leq \pi$$

$$x = \int_0^\theta p(\theta) \, d \cos \theta$$

$$= \int_0^\theta \frac{3}{8} (1 + \cos^2 \theta) \, d \cos \theta$$

$$= -\frac{3}{8} \left(\cos \theta + \frac{\cos^3 \theta}{3} \right) \Big|_0^\theta$$

$$x = -\frac{3}{8} \left(\cos \theta + \frac{\cos^3 \theta}{3} \right) + \frac{1}{2}$$

Now solve for $\cos \theta$.

$$\cos^3 \theta + 3 \cos \theta + (8x - 4) = 0$$

Let

$$y = \cos \theta$$

$$b = 8x - 4$$

$$a = 3$$

$$y^3 + ay + 6 = 0$$

(See Reference 31 for the solution to a cubic equation.)

$$y = A + B$$

or

$$y = -\frac{A+B}{2} + \frac{A-B}{2}\sqrt{-3}$$

or

$$y = -\frac{A+B}{2} - \frac{A-B}{2}\sqrt{-3}$$

where

$$A = \sqrt[3]{-\frac{b}{2} + \sqrt{\frac{b^2}{4} + \frac{a^3}{27}}}$$

and

$$B = \sqrt[3]{-\frac{b}{2} - \sqrt{\frac{b^2}{4} + \frac{a^3}{27}}}$$

Now

$$\frac{b^2}{4} + \frac{a^3}{27} = \frac{b^2}{4} + \frac{3^3}{27} = \frac{b^2}{4} + 1$$

$$\frac{b^2}{4} \geq 0; \quad \frac{b^2}{4} + 1 > 0$$

Therefore, only one real root and two conjugate imaginary roots exist.

Since $y = \cos \theta$, only one real root is considered.

$$\theta = \cos^{-1}(A + B)$$

where

$$A = \sqrt[3]{-\frac{b}{2} + \sqrt{\frac{b^2}{4} + 1}}$$

$$B = \sqrt[3]{-\frac{b}{2} - \sqrt{\frac{b^2}{4} + 1}}$$

and

$$b = 8x - 4$$

APPENDIX C

SAMPLE CALCULATION FOR RANGE PREDICTION

PROBLEM: Given a single channel 280 nm laser utilizing pulse position with power output per pulse equal to one millijoule, determine the communication pattern for a S/N equal to ten. Assume the detector characteristics presented in Section VI.

SOLUTION: From Table V, the minimum photon flux for a S/N of ten is 1.6×10^3 photons per cm^2 .

Now,

$$1 \text{ watt} = 5.0345 \times 10^{18} \lambda \frac{\text{photons}}{\text{sec}}$$

where

$$\lambda = .280 \mu \text{ (}\lambda \text{ is measured in } \mu\text{)}$$

$$1 \text{ joule} = 1 \text{ watt sec}$$

$$= 1.40966 \times 10^{18} \text{ photons}$$

$$1 \text{ millijoule} = 1.40966 \times 10^{15} \text{ photons}$$

From Figure 9, at contour 2 the relative flux is 10^{-2} of the initial photons per unit area where the unit area is one extinction length squared. From Table III one extinction length is

$(1.0405 \text{ km}^{-1})^{-1}$ or .9611 kilometers. The relative flux is $1.0826 \times 10^{-12} \text{ cm}^{-2}$. The irradiance is given by the product of 1.40966×10^{15} and 1.0826×10^{-12} or 1526 photons per square cm. By measuring the distance from the source to the detector located on contour 2 (Figure 9) and recalling that one extinction length for this case is .9611 km, the ranges for an irradiance of $1526 \text{ photons/cm}^2$ may be determined. Table VI lists the results of this calculation.

APPENDIX D

CHECKS ON POSSIBLE ERRORS

Each computational procedure involved in writing this program was verified and an effort was made to ensure the entire program functioned properly. The procedures utilized to document the correct behavior of this routine are described in this appendix.

The various weighting functions in the program were verified by comparing the actual distribution of photons generated by the computer to the analytical solution for the distribution of random numbers obtained using a programmable calculator. (The statements required for this generation remain in the program, but the output of the results is suppressed.)

Verification of axis transformation computations was simple and straight-forward. The axes were rotated about the Z axis, the Y axis, and finally about both axes to ensure proper behavior. (No documentation steps of this nature have been left in the program.) The output of θ , ϕ , θ' , and ϕ' for each photon at each shell was ordered by a computer sort routine in order to facilitate the preparation of a scatter diagram indicating the pattern formed by the simulated photons. Inspection of such a pattern did in fact reveal the presence of a fault which was corrected.

The results of Duntley [32] in describing multiply scattered radiation in the propagation of laser light under water are most useful. Flux as a function of cone angle is presented for distances of up to 19 attenuation lengths. The scattering phase function for light underwater is a sharply peaked function which may be approximated with a Henyey-Greenstein function with a g value equal to 0.96 [33]. Calculations of photon flux as a function of cone angle were carried out with the computer program developed. Total attenuation of the beam down to a level of 10^{-3} could be calculated with some measure of accuracy (only 10,000 simulated photons were utilized for these calculations.) The results of these calculations agreed with the behavior observed in these underwater scattering measurements, simulating correctly the flux levels out to 16 attenuation lengths (the limit calculated).

Further verification of the accuracy of the program was obtained by comparison with calculations by Zachor and Green [24]. In this article, photon flux as a function of viewing angle was calculated for several distances from the source. The same conditions were assumed with the model used here, resulting in satisfactory agreement with the information published by Zachor for distances of 1.43, 2.73, and 4.95 extinction lengths for 300 nm radiation.

APPENDIX E

PROGRAM DESCRIPTION AND DOCUMENTATION

A. COMPONENTS OF THE PROGRAM

1. Weighting Function Subprograms

RANEXP is a function subprogram that generates random numbers weighted exponentially. It is used for distance calculations.

Function subprogram RANTH generates random values for theta and theta prime. Since the interaction may be either Rayleigh scattering or particulate scattering, either calculation may be performed. A uniform random number (generated by RANDU) within the interval $[0,1]$ is obtained and compared to R_p (the ratio of particulate to total scattering). If the random number is less than R_p the particulate scattering calculation is made. (Otherwise the Rayleigh calculation is performed.) Due to the complexity of the particulate phase function it is difficult to obtain an exact solution; therefore, an iterative method is employed. An exact solution is available when f is set to zero and a more efficient calculation is utilized.

RANPH generates a random value of phi or phi prime uniformly weighted on the interval $[0,2\pi]$. The steps in this function subprogram are trivial.

2. LITE Subroutine

The main subroutine of the Monte Carlo simulation, called LITE, simulates a photon which randomly interacts with atmospheric constituents. (In order to make the most efficient use of computer time, non-interaction was not considered.) Initially the photon travels along the $-K_0$ axis (see Figure 16, Appendix A), a distance ΔR (determined by function subprogram RANEXP). A uniform random variable in the interval $[0,1]$ is compared to R_S (the ratio of the total scattering coefficient, K_S , to the total extinction coefficient, K). If the random number is smaller than R_S , the photon is scattered. (Otherwise it is absorbed and the photon is lost.) If it is scattered, the distance of the photon from the laser is updated and a new value of R is calculated. Since the photon has been scattered, new angles and distances must be computed. This is accomplished by generating values for $\Delta\theta$, $\Delta\phi$, and ΔR (using RANTH, RANPH, and RANEXP, respectively). The photon coordinate system is transformed (translated and rotated) to a new coordinate system. The distance from the source is calculated and compared with the radius of a shell. (A series of concentric shells with radii measured in extinction lengths, may be formed in order to determine the photon flux or angular distribution of photons as a function of distance from the source.) Various calculations are then made to determine whether a photon has penetrated through a shell, passed in and out of a shell, or penetrated an outer shell. These calculations are necessary to ensure proper accounting of

the photon flux. When a photon passes through a shell, the position of the source with respect to the penetration point is obtained. Theta, phi, and the radius of the shell (measured in extinction lengths) are stored in a three dimensional array for future use. Theta prime and phi prime are also determined as a function of distance (using RANTH and RANPH). These too, are stored in a three dimensional array and specify the direction of incident photon flux as observed by a receiver located a given distance from the source at a given angle off from the axis of propagation. This process is repeated until all of the photons have been used to generate information. (It should be noted that many extra steps incorporated to debug the program, remain in to facilitate future implementation by another user.)

3. DRLITE Routine

The routine DRLITE is used to drive the subroutine LITE. Information is read into the computer and the results are written out using this routine. The spatial distribution of photons as a function of position and detector field of view is calculated as well as the total number of photons in each shell. The output of other available information is optional and is controlled by IPRT and METHOD statements. This information includes pulse spreading (or photon time of arrival) as a function of position and field of view, the relative photon flux at each annular ring in a shell,

and a least square curve fitting of a modified Henyey-Greenstein function to the phase function information generated by the computer.

4. Miscellaneous Subroutines and Function Subprograms

LSTHG, LEAST, GAUSS3, and RANDU are miscellaneous subroutines used in the program. LSTHG is used to least squares fit a modified Henyey-Greenstein function to the information generated. LEAST and GAUSS3 are used in conjunction with LSTHG. EQN is a function subprogram supporting LSTHG. RANDU is a uniform random number generator that provides numbers in the interval $[0,1]$. It is located in the computer library. The variable IX is the seed and may be any odd integer with nine digits or less. It may not be zero. In order to use RANDU the following FORTRAN statements are used:

```
IX = 948752759  
CALL RANDU (IX,IY,Y)  
IX = IY .
```

The seed IX is used in the calculation and a new seed IY is generated for future use. A uniform random number, Y, is in the interval $[0,1]$ and is also available for future calculations. The last statement ($IX = IY$) resets the seed IX to a new value.


```

440 FCRMAT(IX,'TOTAL NUMBER IN SHELL ',I2,' IS ',I6)
    IF(NFLDVW.EC.1) GC TO 47
DC 46 J=1,NTHETA
ISUM = 0
DC 45 K=1,NFLDVW
    ISUM = ISUM + BINS(I,J,K)
    WRITE(6,441) J,ISUM
441 FCRMAT(,NO. IN BIN ',I2,' IS',I6)
    WRITE(6,521)(BINS(I,J,K),K=1,NFLDVW)
442 CCNTINUE
    GO TO 48
47 WRITE(6,521) ((BINS(I,J,K), K = 1,NFLDVW), J = 1,NTHETA)
48 CCNTINUE
    IF(IPRT.LE.2) GO TO 50
    WRITE(6,442)
442 FCRMAT(/,TIME OF ARRIVAL BINS GIVEN BY',/)
    GO 45 J = 1,NTHETA
49 WRITE(6,522) (BINDST(I,J,K), K = 1,20)
522 FCRMAT(IX,2CI6)
50 CCNTINUE
    IF(IPRT.GE.6) GO TC 399
    IF(IPRT.LT.1) GO TO 1
    WRITE(6,450)
450 FCRMAT(/,THE NEGATIVE LOG CF RELATIVE FLUX AT EACH',
    * ANNUAL RING IS')
DC 60 I = 1,ASHLS
R = DISTSH#I
DO 55 J = 1,NTHETA
    TH1 = (PI*(J-1))/NTHETA
    IF(METHOD.EC.3) TH1 = (TH1*(J-1))/NTHETA
    TH2 = (PI*J)/NTHETA
    IF(METHOD.EC.3) TH2 = (TH2*J)/NTHETA
    AREA = 2.0*PI*R**2*(COS(TH1)-COS(TH2))
    WRITE(7,999) J,AREA
    FCRMAT(,FOR SHELL ',I2,' THE AREA IS',F10.6)
CP 999
    CC 55 K = 1,NFLDVW
    IF(BINS(I,J,K).EQ.0) RFLUX(I,J,K) = 0.0
    IF(BINS(I,J,K).EQ.0) GO TO 55
    RFLUX(I,J,K) = -ALCG10(BINS(I,J,K)/(AREA*NPCT))
55 CCNTINUE
    WRITE(6,452) ((RFLUX(I,J,K), K = 1,NFLDVW),J = 1,NTHETA)
452 FCRMAT(IX,20F6.2)
60 CCNTINUE
521 FCRMAT(IX,2CI6)
    GO TC 1
399 IF(IPRT.LE.5) GO TC 1
400 CC CALL LSTHG(NTHETA,NN,BINS,METHOD,GIN)
    GC TO 1

```

DRL00C490
 DRL000500
 DRL000510
 DRL000520
 DRL000530
 DRL000540
 DRL000550
 DRL000560
 DRL000570
 DRL00C580
 DRL000590
 DRL000600
 DRL000610
 DRL000620
 DRL000630
 DRL000640
 DRL000650
 DRL000660
 DRL000670
 DRL000680
 DRL000690
 DRL000700
 DRL000710
 DRL000720
 DRL000730
 DRL000740
 DRL000750
 DRL000760
 DRL000770
 DRL000780
 DRL000790
 DRL000800
 DRL000810
 DRL000820
 DRL000830
 DRL000840
 DRL000850
 DRL000860
 DRL000870
 DRL000880
 DRL000890
 DRL000900
 DRL000910
 DRL000920
 DRL000930
 DRL000940
 DRL000950
 DRL000960

DRL0097C

END

```

C*****
FUNCTION RANEXP(IX,IY,TAU)
THIS FUNCTION GENERATES A RANDOM NUMBER WEIGHTED EXPONENTIALY
CALL RANDU(IX,IY,RN)
IX = IY
RANEXP = -TAU*ALOG(1.0-RN)
RETURN
END
C
C*****
FUNCTION RANTH(IX,IY,HENA,HENB,HENC,HEND,RPT,FBACK)
THIS FUNCTION GENERATES A RANDOM VALUE OF THETA,
SUITABLY WEIGHTED
DATA PI2/1.5707963268/, PI/3.1415926536/
CALL RANDU(IX,IY,RN)
IX = IY
IF(RN.GT.RPT) GO TO 20
IF(FBACK.EQ.0.0) GO TO 10
CALL RANDU(IX,IY,RN)
IX = IY
CRANM1 = 0.C
LC 5 I = 1,E
CRANTH = HENA-HENB/(RN-HENC-HEND*FBACK*CRANM1*(1.0-CRANM1**2))**2
WRITE(6,999) I,CRANTH,RN
FCRMAT(IX,I4,2F12.6)
IF(ABS(CRANTH-CRANM1).LT.0.001) GO TO 8
CRANM2 = CRANM1
CRANM1 = CRANTH
CONTINUE
CRANTH = 0.25*(CRANM2+CRANTH)+0.5*CRANM1
WRITE(7,998) CRANTH,RN
FCRMAT(IX,2F10.6)
CONTINUE
IF(ABS(CRANTH).GT.1.0) CRANTH = CRANTH/(ABS(CRANTH) + .00001)
RANTH = ARCCS(CRANTH)
RETURN
C*****
1C CALCULATE THETA USING FORWARD SCATTER FUNCTION HERE
CALL RANDU(IX,IY,RN)
IX = IY
WRITE(6,990) HENA,HENB,HENC, RN
FCRMAT(IX,4F12.6)
RANTH = ARCCS(HENA-HENB/(HENC-RN)**2)
RETURN
C*****
20 CALCULATE THETA ASSUMING RAYLEIGH SCATTERING HERE
CALL RANDU(IX,IY,RN)
IX = IY
RLB = 4.0*RN-2.0
RLBS = SQRT(RLB**2+1.0)
CAPA = (-RLB+RLBS)**(1./3.)
CAPB = -(RLB+RLBS)**(1./3.)

```

```

FUN00010
FUN00020
FUN00030
FUN00040
FUN00050
FUN00060
FUN00070
FUN00080
FUN00090
FUN00100
FUN00110
FUN00120
FUN00130
FUN00140
FUN00150
FUN00160
FUN00170
FUN00180
FUN00190
FUN00200
FUN00210
FUN00220
FUN00230
FUN00240
FUN00250
FUN00260
FUN00270
FUN00280
FUN00290
FUN00300
FUN00310
FUN00320
FUN00330
FUN00340
FUN00350
FUN00360
FUN00370
FUN00380
FUN00390
FUN00400
FUN00410
FUN00420
FUN00430
FUN00440
FUN00450
FUN00460
FUN00470
FUN00480

```

```

C
C***
RANTH = ARCCS(CAPA+CAPB)
RETURN
END
FUNCTION RANPH(IX,IY)
THIS FUNCTION GENERATES A RANDOM VALUE OF PI
DATA TPI/6.283183072/
CALL RANDU(IX,IY,RN)
IX = IY
RANPH = TPI*RN
RETURN
END

```

```

FUNCC49C
FUN00500
FUN00510
FUN00520
FUN00530
FUN00540
FUN00550
FUN00560
FUN00570
FUN00580
FUN00590
FUN00600

```



```

C C
      SHELL RELATIVE TO TOTAL DISTANCE A PHOTON
      TRAVELS AFTER A COLLISION
      SLROUTINE LITE(NPHOT,NTHETA,NFLDVW,NSHLS,DISTSH,RATIO,
      *G,RPT,FBACK,IX,BINS,BINDST,METHCC,IPRT)
      INTEGER#4 BINS(20,50,1),BINDST(2C,50,20)
      DIMENSION X(4),Y(4),Z(4),XT(4),YT(4),ZT(4),XS(4),
      *YS(4),ZS(4),RSHL(20),VX(3),VY(3),VZ(3)
      DATA PI/3.1415926536/,TPI/6.2831853072/,RCGTPI/1.772453851/
      DATA EPSIL/1.00E-03/
      WRITE(6,888)
      FCFORMAT(6,888) ENTERED LITE!!
      *WRITE(6,980) NPHOT,NTHETA,NFLDVW,NSHLS,IPRT,METHOD,DISTST,
      *RATIO,G,RPT,FBACK,IX
      *FCFORMAT(1H1,'I2,/,',NTHETA = 'I5',NTHETA = 'I3',NFLDVW = 'I3,
      **NSHLS = 'I2,/,',METHOD = 'I2I1',DISTSH = 'F5.3,
      **RATIO = 'F6.4',G = 'F7.5',RPT = 'F7.5,
      **FBACK = 'F7.5',IX = 'I1C)
      HENA = (1.0+G**2)/(2.0*G)
      HENB = (1.0-G**2)**2/(8.0*G**3)
      HENC = (G+1.0)/(2.0*G)
      HEND = (1.0-G**2)/(4.0*(1.0+G**2)**1.5)
      C**** INITIALIZE ARRAYS
      DC 5 I = 1,NSHLS
      DC 5 J = 1,NTHETA
      DC 4 K = 1,20
      4 BINDST(I,J,K) = 0
      6 CC 6 K = 1,NFLDVW
      5 CCINS(I,J,K) = 0
      C CONTINUE
      NLP = NSHLS+1
      DC 10 I = 1,NUP
      C = D+DISTSH
      1C RSHL(I) = D
      C**** START LOOP FOR EACH PHOTON
      DC 100 NPH = 1,NPHCT
      IXS = IX
      INSCA = 0.0
      RTCT = 0.0
      ISAV = 1
      CC 15 I = 1,4
      X(I) = 0.0
      Y(I) = 0.0
      Z(I) = 0.0
      15 Z(I) = 0.0
      X(2) = 1.0
      Y(4) = 1.0
      Z(3) = 1.0
      C**** CHOOSE DISTANCE OF INITIAL PHOTON

```

```

DRLC0C49C
DRLC0C50C
DRLC0C51C
DRLC0C52C
DRLC0C53C
DRLC0C54C
DRLC0C55C
DRLC0C56C
DRLC0C57C
DRLC0C58C
DRLC0C59C
DRLC0C60C
DRLC0C61C
DRLC0C62C
DRLC0C63C
DRLC0C64C
DRLC0C65C
DRLC0C66C
DRLC0C67C
DRLC0C68C
DRLC0C69C
DRLC0C70C
DRLC0C71C
DRLC0C72C
DRLC0C73C
DRLC0C74C
DRLC0C75C
DRLC0C76C
DRLC0C77C
DRLC0C78C
DRLC0C79C
DRLC0C80C
DRLC0C81C
DRLC0C82C
DRLC0C83C
DRLC0C84C
DRLC0C85C
DRLC0C86C
DRLC0C87C
DRLC0C88C
DRLC0C89C
DRLC0C90C
DRLC0C91C
DRLC0C92C
DRLC0C93C
DRLC0C94C
DRLC0C95C
DRLC0C96C

```

```

DR = RANEXP(IX,IY,1.0)
DC 17 I = 1,4
17 Z(I) = Z(I) + DR
18 IF(DR.LT.RSHL(ISAV+1)) GO TC 19
ISAV = ISAV+1
IF(ISAV.GT.NSHLS) GC TO 100
GC TO 18
CONTINUE
19 RTOT = DR
SCIST = RTOT
DETERMINE IF PHOTON IS ABSORBED OR SCATTERED
C****
2C CALL RANDU(IX,IY,RN)
IX = IY
IF(RN.GT.RATIO) GC TO 100
IF PHOTON IS SCATTERED, DETERMINE NEW ANGLES AND DISTANCES
C****
NSCA = NSCA+1
DR = RANEXP(IX,IY,1.0)
DTHETA = RANRTH(IX,IY,HENA,HENB,HENC,HEND,RPT,FBACK)
DPHI = RANRPH(IX,IY)
STH = SIN(DTHETA)
SPH = CCS(DTHETA)
CPH = CCS(DPHI)
WRITE(6,990) RTOT,DR,DTHETA,DPHI,STH,CTH,SPT,CPH
CP 99C * 1X,8F10.5)
FCRMTAT(IX,8F10.5)
C****
RTOT = NEW PHOTON POSITION AND TRANSLATE
DO 30 I = 1,4
XT(I) = X(I)*CTH*SPT-Y(I)*CTH*SPT-Z(I)*STH
YT(I) = X(I)*SPH + Y(I)*CPH
ZT(I) = X(I)*STH*CPT - Y(I)*STH*SPT + Z(I)*CTH + DR
CP 991 * 1X,8F10.5)
FCRMTAT(IX,8F10.5)
C****
DIST = SQRT(XT(1)**2+YT(1)**2+ZT(1)**2)
CHECK TO SEE IF PHOTON HAS PENETRATED A SHELL
CONSIDER IF PHOTON HAS PENETRATED IN AND OUT OF SHELL
FF IS FRACTIONAL DISTANCE BETWEEN TWO POINTS GIVING
FF THE DISTANCE OF CLOSEST APPROACH
FF = 1.0-ZT(1)/DR
IF((FF.LT.0.0).OR.(FF.GT.1.0)) GC TO 35
DC IS DISTANCE OF CLOSEST APPROACH
DC = SQRT(XT(1)**2+YT(1)**2)
C****
IF(DC.GT.RSHL(ISAV)) GO TO 35
ISAV = ISAV+1
WRITE(7,920) DC,RSHL(ISAV),FF,IX
CP 920 * 1X,3F10.5,1X,I10)
FCRMTAT(IX,3F10.5,1X,I10)
IF(DC.GT.RSHL(ISAV)) GO TO 50

```

DRLCC97C
 DRL00980
 DRLCC990
 DRL01000
 DRL01010
 DRL01020
 DRL01030
 DRL01040
 DRL01050
 DRL01060
 DRL01070
 DRL01080
 DRL01090
 DRL01100
 DRL01110
 DRL01120
 DRL01130
 DRL01140
 DRL01150
 DRL01160
 DRL01170
 DRL01180
 DRL01190
 DRL01200
 DRL01210
 DRL01220
 DRL01230
 DRL01240
 DRL01250
 DRL01260
 DRL01270
 DRL01280
 DRL01290
 DRL01300
 DRL01310
 DRL01320
 DRL01330
 DRL01340
 DRL01350
 DRL01360
 DRL01370
 DRL01380
 DRL01390
 DRL01400
 DRL01410
 DRL01420
 DRL01430
 DRL01440

```

C*** 25 GC TO 35
C*** 26 CC CONSIDER IF PHOTON HAS PENETRATED CUTER SHELLS
C*** 27 IF((ISAV).GT.(NSHLS)) GO TO 100
C*** 28 IF(DIST.GT.RSHL(ISAV+1)) GO TO 5C
C*** 29 IF(DIST.GT.RSHL(ISAV)) GO TO 40
C*** 30 ISAV = ISAV-1
C*** 31 GO TO 37
C*** 32 TIME TO 37 UPDATE COORDINATES - GET READY FOR ANOTHER COLLISION
C*** 33 RTCT = RTGT+DR
C*** 34 SCIST = DIST
C*** 35 CC 45 I = 1,4
C*** 36 X(I) = XT(I)
C*** 37 Y(I) = YT(I)
C*** 38 Z(I) = ZT(I)
C*** 39 CC CONTINUE
C*** 40 GO TO 20 FOR ANOTHER COLLISION
C*** 41 GC TO 20
C*** 42 CALCULATE CCORDINATES OF POINT AT WHICH PHOTON PENETRATES SHELL
C*** 43 ISAV = ISAV+1
C*** 44 CP 551 WRITE(6,551) DR,ZT(1) **,2F10.5)
C*** 45 FCRMAT(,**** DR,ZT(1) **,2F10.5)
C*** 46 CP 552 WRITE(6,552) SDIST,RSHL(ISAV) **,2F10.5)
C*** 47 FCRMAT(,**** SDIST,RSHL(ISAV) **,2F10.5)
C*** 48 CP 553 WRITE(6,553) DIST,RTOT,ISAV **,2F10.5,2X,I2)
C*** 49 FCRMAT(,**** DIST,RTOT,ISAV **,2F10.5,2X,I2)
C*** 50 XPDR = (DR-ZT(1)+SQRT((ZT(1)-DR)**2-SDIST**2+RSHL(ISAV)**2))/CR
C*** 51 WRITE(6,550) XPDR = ,F10.5)
C*** 52 FCRMAT(, XPDR = ,F10.5)
C*** 53 DC 55 I = 1,4
C*** 54 XS(I) = XT(I)
C*** 55 YS(I) = YT(I)
C*** 56 ZS(I) = ZT(I) - (1.0-XPDR)*DR
C*** 57 CC CONTINUE
C*** 58 PDIST = RTOT+XPDR*DR
C*** 59 CP 992 WRITE(6,992) (XS(I),YS(I),ZS(I), I = 1,4)
C*** 60 FCRMAT(, COCRD. AT SHELL: ,12F9.5)
C*** 61 CALCULATE VALUE OF THETA
C*** 62 VAL = ((XS(1)*(XS(1)-XS(3)) + YS(1)*(YS(1)-YS(3))
C*** 63 + ZS(1)*(ZS(1)-ZS(3)))/RSHL(ISAV))
C*** 64 * IF(ABS(VAL).GT.1.1) CALL PERR(1,IXS,VAL,XS,YS,ZS)
C*** 65 IF(ABS(VAL).GT.1.1) WRITE(6,200) VAL,NPH,IXS
C*** 66 FCRMAT(, ARCOS GT. 1.1; VAL = ,F10.5, NPH = ,IX = ,
C*** 67 I10)
C*** 68 IF(VAL.GT.1.0) VAL = 1.0
C*** 69 IF(VAL.LT.-1.0) VAL = -1.0
C*** 70 TH = PI - ARCOS(VAL)
C*** 71 IF(TH.LT.0.0) TH = 0.0
C*** 72 WRITE(6,999) RSHL(ISAV)
C*** 73 CP

```

```

995 FCRMAT(, AAA, F10.5)
C**** CALCULATE VALUE OF PHI
      DENOMS = (RSHL(1SAV)**2 - (XS(1)*(XS(3)-XS(1)) + YS(1)*
      * (YS(3)-YS(1)) + ZS(1)*(ZS(3)-ZS(1)))**2)
      IF(DENOMS.LT.-EPSIL) CALL PERR(5, IXS, DENOMS, XS, YS, ZS)
      IF(DENOMS.LT.-EPSIL) DENOMS = 0.0
      DENOM = SQRT(DENOMS)
      WRITE(6, 996) DENOM, IXS
      IF(DENOM.EQ.0.0) PH = 0.0
      IF(DENOM.EQ.0.0) GO TO 158
996 FCRMAT(, DENOM: , F10.6, I10)
      * VAL = ((XS(1)*(XS(1)-XS(2)) + YS(1)*(YS(1)-YS(2)) +
      * ZS(1)*(ZS(1)-ZS(2)))/DENOM)
      IF(ABS(VAL).GT.1.1) CALL PERR(2, IXS, VAL, XS, YS, ZS)
      IF(ABS(VAL).GT.1.1) WRITE(6, 200) VAL, NPH, IXS
      IF(VAL.GT.1.0) VAL = 1.0
      IF(VAL.LT.-1.0) VAL = -1.0
      PH = ARCCOS(VAL)
      IF((XS(1)*(XS(1)-XS(4))+YS(1)*(YS(1)-YS(4))+ZS(1)*(ZS(1)-ZS(4)))
      *).LT.0.0) PH = TPI-PH
158 CONTINUE
CP      WRITE(6, 998)
998 FCRMAT(, BBB, )
C**** CALCULATE VALUE OF THETA PRIME (RECEIVER)
      VAL = (ZS(1)/RSHL(1SAV))
      IF(ABS(VAL).GT.1.1) CALL PERR(3, IXS, VAL, XS, YS, ZS)
      IF(ABS(VAL).GT.1.1) WRITE(6, 200) VAL, NPH, IXS
      IF(VAL.GT.1.0) VAL = 1.0
      IF(VAL.LT.-1.0) VAL = -1.0
      THP = ARCCS(VAL)
      WRITE(6, 997)
997 FCRMAT(, CCC, )
C**** CALCULATE VALUE OF PHI PRIME (RECEIVER)
      PARAM = (XS(1)*XS(3) + YS(1)*YS(3) + ZS(1)*ZS(3))/
      * (RSHL(1SAV)*SQRT(XS(2)**2 + YS(2)**2 + ZS(2)**2))
      WRITE(6, 911) IXS, PARAM
911 FCRMAT(, IXS, PARAM = , I10, E12.6)
      IF(PARAM.LT.0.999) GO TO 159
      VAL = XS(2)-XS(1)
      GC TO 585
159 BP = -RSHL(1SAV)**2/(XS(3)*XS(1)+YS(3)*YS(1)+ZS(3)*ZS(1))
      VX(1) = XS(1)+BP**XS(3)
      VY(1) = YS(1)+BP**YS(3)
      VZ(1) = ZS(1)+BP**ZS(3)
      ANORM = SQRT(VX(1)**2+VY(1)**2+VZ(1)**2)
      VX(1) = VX(1)/ANORM
      VY(1) = VY(1)/ANORM
      VZ(1) = VZ(1)/ANORM

```

DR L0193C
 DR L01940
 DR L01950
 DR L01960
 DR L01970
 DR L01980
 DR L01990
 DR L02000
 DR L02010
 DR L02020
 DR L02030
 DR L02040
 DR L02050
 DR L02060
 DR L02070
 DR L02080
 DR L02090
 DR L02100
 DR L02110
 DR L02120
 DR L02130
 DR L02140
 DR L02150
 DR L02160
 DR L02170
 DR L02180
 DR L02190
 DR L02200
 DR L02210
 DR L02220
 DR L02230
 DR L02240
 DR L02250
 DR L02260
 DR L02270
 DR L02280
 DR L02290
 DR L02300
 DR L02310
 DR L02320
 DR L02330
 DR L02340
 DR L02350
 DR L02360
 DR L02370
 DR L02380
 DR L02390
 DR L02400

DRLO2410
DRLO2420
DRLO2430
DRLO2440
DRLO2450
DRLO2460
DRLO2470
DRLO2480
DRLO2490
DRLO2500
DRLO2510
DRLO2520
DRLO2530
DRLO2540
DRLO2550
DRLO2560
DRLO2570
DRLO2580
DRLO2590
DRLO2600
DRLO2610
DRLO2620
DRLO2630
DRLO2640
DRLO2650
DRLO2660
DRLO2670
DRLO2680
DRLO2690
DRLO2700
DRLO2710
DRLO2720
DRLO2730
DRLO2740
DRLO2750
DRLO2760
DRLO2770
DRLO2780
DRLO2790
DRLO2800
DRLO2810
DRLO2820
DRLO2830
DRLO2840
DRLO2850
DRLO2860
DRLO2870
DRLO2880

```

CP 585      XS(1)/RSHL(ISAV)
            VS(1)/RSHL(ISAV)
            ZS(1)/RSHL(ISAV)
            VZ(1)-VZ(3)*VY(1)
            VY(2) = VZ(3)*VX(1)-VX(3)*VZ(1)
            VZ(2) = VX(3)*VY(1)-VY(3)*VX(1)
            WRITE(6,989) BP,ANORM,((VX(1),VY(1),VZ(1)),I=1,3)
            FCFORMAT(, BP, ANORM, V(1), V(1), V(1), V(1): ,11F8.4)
            IF(VZ(3).LT.0.9999) GO TO 58
            VAL = 1.0
            GC TO 59
            CCNTINUE
58      VAL = VZ(1)/SQRT(1.0-VZ(3)**2)
            IF(ABS(VAL).GT.1.1) CALL PERR(4,3,RSHL(ISAV),VX,VY,VZ)
            IF(ABS(VAL).GT.1.1) CALL PERR(4,3,XS,VAL,XS,VS,ZS)
            IF(ABS(VAL).GT.1.1) WRITE(6,200) VAL, NPH, IXS
            IF(VAL.GT.1.0) VAL = 1.0
            IF(VAL.LT.-1.0) VAL = -1.0
            PHP = ARCCOS(VAL)
59      IF(VZ(2).LT.0.0) PHP = TPI-PHP
            FCFORMAT(, DDC)
            TALLY LOCATION OF ANGULAR RESULTS
            IF(METHOD.LE.2) NTH = (TH*NTHETA/PI) + 1/RCTPI + 1
            IF(METHOD.GE.3) NTH = (SQRT(TH)*NTHETA)/PI + 1
            IF(METHOD.LE.2) NTHP = 2.0*THP*NFLDVW/PI + 1
            IF(METHOD.GE.3) NTHP = (SQRT(2.0*THP)*NFLCVW)/ROOTPI + 1
            IF(IPRT.NE.9) GO TO 70
            WRITE(9,993)NPH,ISAV,NTH,NSCA,TH,PH,THP,PHP,PDIST
            FCFORMAT(415,4F10.5,F10.5)
            CCNTINUE
            BINS(ISAV-1,NTH,NTHP) = BINS(ISAV-1,NTH,NTHP) + 1
            XXXX = ((YS(3)-YS(1))*ZS(1) - (ZS(3)-ZS(1))*YS(1))*VX(1)
            YZXX = ((ZS(3)-ZS(1))*XS(1) - (XS(3)-XS(1))*ZS(1))*VY(1)
            ZZXX = ((XS(3)-XS(1))*YS(1) - (YS(3)-YS(1))*XS(1))*VZ(1)
            WRITE(6,986)XXX,YYXX,ZZXX
            FCFORMAT(, XXXX, YYXX, ZZXX: ,3F10.6)
            TALLY LOCATION OF INTERSECTION IN DISTANCE CF ARRIVAL BINS
            IF(PDIST.LE.(1.00001*RSHL(ISAV))) PDIST = 1.00001*RSHL(ISAV)
            XCIPDIST = ALOG10((PCDIST/RSHL(ISAV))-1.0) + 4.0
            IF(XDIST.LT.0.0) XDIST = 0.0
            IF(XDIST.GE.4.99) XDIST = 4.99
            NCLIST = (XDIST*20)/5 + 1
            BINDST(ISAV-1,NTH,NDIST) = BINDST(ISAV-1,NTH,NDIST) + 1
            GC TO 35
            CCNTINUE
100      RETURN
            END

```

```

WRITE FUNCTION SUBPROGRAM TO CALCULATE THE FUNCTION TO BE VARIED SUCH AS
A IS DIMENSIONED TO AND CONTAINS THE PARAMETERS TO BE VARIED SUCH AS
MINIMIZE THE SUM OF SQUARES X, XB, AND XC ARE THE THREE INDEP
PARAMETERS (YOU MAY WISH TO USE ONLY X) NOF IS THE FUNCTION NUMBER -
BRANCHING TO DIFFERENT PARTS OF THE EQN SUBPROGRAM WHEN SEVERAL
ARE TO BE FIT (FOR SEVERAL JOBS TO BE DONE).
THE DIMENSIONED ARRAYS HAVE THE FOLLOWING MEANING--
X(200), XB(200), AND XC(200) CONTAIN THE INDEPENDENT PARAMETERS.
Z(200) CONTAINS THE OBSERVED VALUES OF THE FUNCTION (THE OBSERVED
PARAMETERS).
FINCR(10) CONTAINS THE MAGNITUDE OF THE INCREMENTS FOR THE PARAMETERS
SC THAT THE PROGRAM MAY TAKE NUMERICAL DERIVATIVES WITH REASONABLE
R(200) CONTAINS THE DIFFERENCE BETWEEN OBSERVED (Z(200)) AND CALCULATED
E(10) CONTAINS THE ESTIMATES OF THE ERRORS OF THE PARAMETERS A(10)
ITERATION.
INPUT
FIRST CARD - WILL BE REPRODUCED ON OUTPUT USED FOR LABELING.
SECOND CARD FORMAT(I2,I3,I2,I3,E10.2)
IR= NUMBER OF PARAMETERS TO BE VARIED
IS= NUMBER OF POINTS
NOF= FUNCTION NUMBER (SEE ABOVE)
NINP= NUMBER OF INDEPENDENT PARAMETERS
EPSIL= IS USED AS A CRITERION FOR CONVERGENCE. IF THE RELATIVE VALUE
OF THE RESIDUAL CHANGES BY LESS THAN EPSIN IN TWO SUCCESSIVE
CONVERGENCE IS REACHED.
SUBROUTINE LSTHG(IS,NN,IBIN,NOF,XFNIN)
IMPLICIT REAL*8 (A-H,C-Z)
INTEGER*4 IBIN(20,50,1)
DIMENSION A(10), X(200), XB(200), XC(200), Z(200), FINCR(10),
1R(200), E(10)
CALL ERSET(208,0,-1,C,0,0)
DO 2 I=1,IS
Z(I)=IBIN(NN,I,1)
2 SUM=0.0
DO 5 I=1,IS
SUM=SUM+Z(I)
5 IF(SUM.LT.20) RETURN
IR=2
NINP=1
EPSIL=.0001
GG TO (7,8,8), NOF
7 CONTINUE
A(1)=SUM
A(2)=.90
A(10)=180./IS
GC TO 9
8 A(1)=.8

```

CCCCCCCCCCCCCCCCCCCCCCCCCCCCCCCCCCCC


```

C      30      WRITE(6,105)
999      FCRMAT(6,999)
30      CALL LEAST(IR,IS,A,X,XB,XC,Z,FINCF,EPSIL,NCITR,RRQ,NGF,R,E)
30      WRITE(6,106)
      WRITE(6,107)
      WRITE(6,108)
      WRITE(6,109)
      WRITE(6,110)
      WRITE(6,111)
      WRITE(6,112)
      WRITE(6,113)
      WRITE(6,114)
      WRITE(6,115)
      WRITE(6,116)
      WRITE(6,117)
      WRITE(6,118)
      WRITE(6,119)
      WRITE(6,120)
      WRITE(6,121)
      WRITE(6,122)
      WRITE(6,123)
      RETURN
      FCRMAT(12,13,12,13,E10.2)
      FCRMAT(16F5.0)
      FCRMAT(16F5.0)
      FCRMAT(16F5.0)
      FCRMAT(16F5.0)
      FCRMAT(16F5.0)
      FCRMAT(80H)
107 FCRMAT(99H,NUMBER OF PARAMETERS
108 FCRMAT(8X,12,24X,I3,17X,I2,19X,I2,12X,E1C.2)
109 FCRMAT(1H)
110 FCRMAT(26H,THE PARAMETERS FED IN ARE)
111 FCRMAT(1H,10F10.5)
112 FCRMAT(55H,THE INCREMENTS FOR CERTAINING NUMERICAL DERIVATIVES ARE)
113 FCRMAT(34H,THE OBSERVED VALUES TC BE FIT ARE)
114 FCRMAT(1X,10F10.2)
115 FCRMAT(31H,THE INDEPENDENT PARAMETERS ARE)
116 FCRMAT(1H,10F10.5)
117 FCRMAT(1H,10F10.5)
118 FCRMAT(1H,10F10.5)
119 FCRMAT(38H,THE BEST VALUES OF THE PARAMETERS ARE)
120 FCRMAT(1H,7F12.5)
121 FCRMAT(24H,NUMBER OF ITERATIONS = ,I2,50H THE SUM OF THE SQUARES OF THE ERRORS IS NOW = ,E12.6)
122 FCRMAT(53H,OBSERVED MINUS CALCULATED VALUES OF THE BEST FIT ARE)
123 FCRMAT(1H,10F10.2)
124 FCRMAT(66H,ESTIMATES OF THE ERRCR IN EACH PARAMETER ARE (STANDARD

```

```

TGC97C
LST00980
LST00990
LST01000
LST01010
LST01020
LST01030
LST01040
LST01050
LST01060
LST01070
LST01080
LST01090
LST01100
LST01110
LST01120
LST01130
LST01140
LST01150
LST01160
LST01170
LST01180
LST01190
LST01200
LST01210
LST01220
LST01230
LST01240
LST01250
LST01260
LST01270
LST01280
LST01290
LST01300
LST01310
LST01320
LST01330
LST01340
LST01350
LST01360
LST01370
LST01380
LST01390
LST01400
LST01410
LST01420
LST01430
LST01440

```

```

1  DEVIATION) )
200 STOP
END
C
C SUBROUTINE LEAST(IR,IS,A,X,XB,XC,Z,FINCR,EPSIL,NOITR,RRQ,NOF,R,E)
C IMPLICIT REAL*8 (A-H,C-Z)
C IR = NO. OF PARAMETERS, IS = NO. OF PCINTS, A IS ARRAY CF PARAMETERS,
C X IS INDEPENDENT VARIABLE( Z DEPENDENT. FINCR IS ARRAY OF INCREMENTS,
C PARAMETERS EPSIL IS -FRACTIONAL- ERROR CRITERION. NOITR IS NO. OF
C ITERATIONS. REQUIRED (UP TO 10). RRQ = SUM OF SQUARES CF RESIDUALS)
C NCF IS NUMBER CF THE FUNCTION USED IN -EQN-.
C E IS THE ARRAY CF ESTIMATED ERRORS IN THE PARAMETERS
C DIMENSION A(10), X(200), XB(200), XC(200), Z(200), FINCR(10), R(200),
C 10) D(200,10), DT(10,200), DEL(10), DS(10), CPI(10,10),
C 2E(10)
C NCITR = 0
C DC 20 I = 1,IS
C R(I) = Z(I) - EQN(A,X(I),X(I+1),XC(I),NOF)
C IF (NOITR-9) 130,130,4
C NCITR = NOITR + 1
C DC 220 J = 1,IR
C A(J) = A(J)+FINCR(J)
C DC 15 I = 1,IS
C D(I,J) = EQN(A,X(I),X(I+1),XC(I),NCF)
C A(J) = A(J)-FINCR(J)
C 220 CONTINUE
C DC 30 I = 1,IS
C CCNST = EQN(A,X(I),X(I+1),XC(I),NCF)
C DC 30 J = 1,IR
C C(I,J) = (D(I,J)-CONST)/FINCR(J)
C DC 35 I = 1,IS
C DC 35 J = 1,IR
C DT(J,I) = D(I,J)
C DC 598 I = 1,IR
C WRITE(6,999) (DT(I,J), J = 1,IS)
C 999 FORMAT(1X,12F10.5)
C DC 36 I = 1,IR
C DC 36 J = 1,IR
C DP(I,J) = 0.0
C DC 36 K = 1,IS
C C(I,J) = DP(I,J)+DT(I,K)*D(K,J)
C CALL GAUSS3 (IR,1.00E-30,DP,DPI,KER)
C IF (KER-1) 120,37,120
C DC 40 I = 1,IS
C DC 38 J = 1,IR
C DS(J) = 0.0
C DC 38 K = DS(J)+DPI(J,K)*DT(K,I)
C DS(J) = DS(J)

```

```

      39 L = 1,IR
      DT(L,I) = DS(L)
      CCNTINUE
      DC 993 I = 1,IR
      WRITE(6,992) (DPI(I,J), J = 1,IR)
      FORMAT(IX,12F10.5)
      DC 990 I = 1,IR
      WRITE(6,991) (DT(I,J), J = 1,IS)
      WFORMAT(IX,1CE12.4)
      DC 991 I = 1,IR
      WRITE(6,991) (R(I), I = 1,IS)
      DEL(I) = 0.0
      DC 110 J = 1,IS
      DEL(I) = DEL(I)+DT(I,J)*R(J)
      DC 110 I = 1,IR
      A(I) = A(I)+DEL(I)
      IF(NOF.GE.4) GO TO 222
      IF(NOF.GE.2) GO TO 219
      IF(A(2).GT..99) A(2) = 0.99
      GC TO 222
      219 IF(A(1).GT..99) A(1) = 0.99
      IF(A(2).LT.0.3) A(2) = 0.3
      CCNTINUE
      DC 320 I = 1,IS
      R(I) = Z(I) - EQN(A,X(I),X(I+1),XC(I),NOF)
      RRQ = 0.0
      CC 50 I = 1,IS
      RRQ = RRQ+R(I)*#2
      WRITE(6,102) (A(I), I = 1,IR), RRQ
      102 WFORMAT(1H,10E12.4)
      CRRES = DABS(RRQ-RRP) - EPSIL*RRP
      RRP = RRQ
      IF(CRES) 100,100,25
      IF(CRES) 20H CONVERGENCE FAILURE)
      101 WFORMAT(5,101)
      GC TO 100
      120 WRITE(6,1001)
      1001 WFORMAT(16H MATRIX SINGULAR)
      100 FISI = IS-IR
      DC 150 I = 1,IR
      150 E(I) = DSQRT(RRQ*CPI(I,I))
      RETURN
      END
      SUBROUTINE GAUSS3(N,EP,A,X,KER)
      IMPLICIT REAL*8 (A-H,C-Z)
      DIMENSION A(10,10), X(10,10)
      DC 1 I=1, N

```

```

LSTC153C
LSTC154C
LSTC155C
LSTC156C
LSTC157C
LSTC158C
LSTC159C
LSTC160C
LSTC161C
LSTC162C
LSTC163C
LSTC164C
LSTC165C
LSTC166C
LSTC167C
LSTC168C
LSTC169C
LSTC170C
LSTC171C
LSTC172C
LSTC173C
LSTC174C
LSTC175C
LSTC176C
LSTC177C
LSTC178C
LSTC179C
LSTC180C
LSTC181C
LSTC182C
LSTC183C
LSTC184C
LSTC185C
LSTC186C
LSTC187C
LSTC188C
LSTC189C
LSTC190C
LSTC191C
LSTC192C
LSTC193C
LSTC194C
LSTC195C
LSTC196C
LSTC197C
LSTC198C
LSTC199C
LSTC200C
LSTC201C
LSTC202C
LSTC203C
LSTC204C
LSTC205C
LSTC206C
LSTC207C
LSTC208C
LSTC209C
LSTC210C
LSTC211C
LSTC212C
LSTC213C
LSTC214C
LSTC215C
LSTC216C
LSTC217C
LSTC218C
LSTC219C
LSTC220C
LSTC221C
LSTC222C
LSTC223C
LSTC224C
LSTC225C
LSTC226C
LSTC227C
LSTC228C
LSTC229C
LSTC230C
LSTC231C
LSTC232C
LSTC233C
LSTC234C
LSTC235C
LSTC236C
LSTC237C
LSTC238C
LSTC239C
LSTC240C

```

```

1  CC 1 J=1,N
2  DC 1 J)=0.0
10 DC 2 K=1,N
   DC 3 K)=1.0
   DC 4 L=1,N
   KP=0
   Z=C.0
11 DC 12 K=L,N
   IF(Z-DABS(A(K,L)))11,12,12
   Z=CABS(A(K,L))
12 KP=K
12 CCNTINUE
13 IF(L-KP)13,20,20
13 DO 14 J=L,N
   Z=A(L,J)
   A(L,J)=A(KP,J)
14 AC(KP,J)=Z
   AC 15 J=1,N
   Z=X(L,J)
   X(L,J)=X(KP,J)
15 X(KP,J)=Z
20 IF(DABS(A(L,L))-EP)50,50,30
30 IF(L-N)31,34,34
31 LP1=L+1
   DC 36 K=LPI,N
   IF(A(K,L))32,36,32
   RATIO=A(K,L)/A(L,L)
32 DO 33 J=LPI,N
   A(K,J)=A(K,J)-RATIO*A(L,J)
33 AC(K,J)=A(K,J)-RATIO*X(L,J)
35 X(K,J)=X(K,J)-RATIO*X(L,J)
36 CCNTINUE
34 DO 43 I=1,N
   II=N+1-I
   DC 45 J=1,N
   S=0.0
   IF(II-N)41,43,43
41 IPI=I+1
   DC 42 K=IPI,N
   S=S+A(II,K)*X(K,J)
42 X(II,J)=X(II,J)-S/A(II,II)
43 KER=1
50 KER=2
   RETURN
   END

```

```

JSTT02024410
JSTT02024420
JSTT02024430
JSTT02024440
JSTT02024450
JSTT02024460
JSTT02024470
JSTT02024480
JSTT02024490
JSTT02025500
JSTT02025510
JSTT02025520
JSTT02025530
JSTT02025540
JSTT02025550
JSTT02025560
JSTT02025570
JSTT02025580
JSTT02025590
JSTT02026000
JSTT02026010
JSTT02026020
JSTT02026030
JSTT02026040
JSTT02026050
JSTT02026060
JSTT02026070
JSTT02026080
JSTT02026090
JSTT02027000
JSTT02027010
JSTT02027020
JSTT02027030
JSTT02027040
JSTT02027050
JSTT02027060
JSTT02027070
JSTT02027080
JSTT02027090
JSTT02028000
JSTT02028010
JSTT02028020
JSTT02028030
JSTT02028040
JSTT02028050
JSTT02028060
JSTT02028070

```

LST000010
 LST000020
 LST000030
 LST000040
 LST000050
 LST000060
 LST000070
 LST000080
 LST000090
 LST000100
 LST000110
 LST000120
 LST000130
 LST000140
 LST000150
 LST000160
 LST000170
 LST000180
 LST000190
 LST000200
 LST000210
 LST000220
 LST000230
 LST000240
 LST000250
 LST000260
 LST000270
 LST000280
 LST000290
 LST000300
 LST000310
 LST000320

```

REAL FUNCTION HG*8(AMPL,G,XPN,X,DEL)
IMPLICIT REAL*8 (A-H, O-Z)
DATA CR/0.017453/
TNT = 2.0*XFN-2.0
WRITE(6,991) AMPL,G,XPN,X
CP 991 FCFORMAT(1X,4F10.6)
      GS = G*2
      TG = 2.0*G
      QPGS = 1.0+GS
      HG = AMPL*(1.0/((1.0-((1.0-G)**(TNT)))-(1.0/((1.0+G)**(TNT)))))
      1 * (1.0/(OPGS-TG*DCOS(X*CR)))*(XPN-1.0)
      2 - 1.0/(OPGS-TG*DCCS((X+DEL)*CR))*(XPN-1.0)
CP 999 WRITE(6,999) AMPL,G,HG,X
      FCFORMAT(1X,2F10.5,E12.4,F10.4)
      IF(INUM.GE.NCF) RETURN
END
REAL FUNCTION EQN*8(A,X,XB,XC,NCF)
IMPLICIT REAL*8 (A-H, O-Z)
DIMENSION A(10)
GO TO (5,55,155,255), NOF
5    DEL = A(10)
      EQN = HG(A(1),A(2),1.5,X,DEL)
      RETURN
55   DEL = A(10)
      EQN = HG(A(9),A(1),A(2),X,DEL)
      RETURN
155  DEL = XB-X
      EQN = HG(A(9),A(1),A(2),X,DEL)
      RETURN
255  EQN = A(1)*X**2 + A(2)*X + A(3)
      RETURN
END
  
```

PER000010
 PER000020
 PER000030
 PER000040
 PER000050
 PER000060
 PER000070
 PER000080
 PER000090
 PER000100
 PER000110
 PER000120

```

SUBROUTINE PERR(ERRNC,IXS,PARAM,XS,YS,ZS)
INTEGER*4 ERRNO
DIMENSION XS(4), YS(4), ZS(4)
NUP = 4
IF(IXS.LT.4) NUP = IXS
WRITE(6,100) ERRNC,PARAM,IXS
FCFORMAT(,ERROR DETECTED, LOCATION NO. ',I5,' PARAM = ',
E14.8, IXS = ',I1C)
100 * WRITE(6,110) (XS(I), YS(I), ZS(I), I = 1,NUP)
11C FCFORMAT(, COCRD. FROM PERR: ',12F9.5)
      RETURN
END
  
```


LIST OF REFERENCES

1. Naval Research Laboratory Report 6152, Experimental Observations of Forward Scattering of Light in the Lower Atmosphere, by J.A. Curcio and L.F. Drummeter, Jr., 30 September 1964.
2. Battelle Memorial Institute Report BAT-171-4, Feasibility of Non-Line-of-Sight Laser Communications, by G.T. Ruck, 15 December 1964.
3. King, M. and Kainer, S., "Some Parameters of a Laser-Type Beyond-the-Horizon Communications Link," Proceedings of the IEEE, v. 53, p. 137-141, February 1965.
4. Naval Electronics Laboratory Center Report 1988 (TR 1988), Extended Line-of-Sight Optical Communications Study, by G.C. Mooradian, V.J. Adrian, P.H. Levine, and W.R. Stone, p. 9, 30 June 1976, changed 4 November 1976.
5. Air Force Cambridge Research Laboratories Report 75-0255, Atmospheric Transmittance from 0.25 to 28.5 μ m: Computer Code LOWTRAN 3, by J.E.A. Selby and R.A. McClatchey, p. 38-44, 7 May 1975.
6. Air Force Cambridge Research Laboratories Report 72-0497, Optical Properties of the Atmosphere, (3rd ed.), by R.A. McClatchey, R.W. Fenn, J.E.A. Selby, F.E. Volz, and J.S. Garing, p. 36-37, 69-71, 24 August 1972.
7. Aeronautical Research Associates of Princeton Report 274, Vol. I, Voice Communication via Scattered Ultraviolet Radiation, by E.S. Fishburne, M.E. Neer, and G. Sandri, February 1976.
8. Aeronautical Research Associates of Princeton Report 285, Voice Communication via Atmospheric Scattering of Ultraviolet Radiation, by E.S. Fishburne and M.E. Neer, July 1976.
9. Bhaumik, M.L., "High Efficiency UV Lasers," Laser Focus, v. 12, p. 55, February 1976.
10. Bhaumik, M.L., Bradford, R.S., Jr., and Ault, E.R., "High Efficiency KrF Eximer Laser," Applied Physics Letters, v. 28, p. 23, 1976.

11. Naval Research Laboratory Memorandum Report 3238, Ultraviolet Extinction Measurements of the Chesapeake Bay, by J.A. Curcio and G.L. Knestrick, p. 12, March 1976.
12. Shettle, E.P. and Green, A.E.S., "Multiple Scattering Calculation of the Middle Ultraviolet Reaching the Ground," Applied Optics, v. 13, p. 1567-1581, July 1974.
13. Stotts, L.B., "The Radiance Produced by Laser Radiation Transversing a Particulate Multiple-Scattering Medium," Journal of the Optical Society of America, v. 67, n. 6, p. 815-819, June 1977.
14. Bucher, E.A., "Computer Simulation of Light Pulse Propagation for Communication Through Thick Clouds," Applied Optics, v. 12, n. 10, p. 2391-2400, October 1973.
15. Bucher, E.A., "Experiments on Light Pulse Communication and Propagation Through Atmospheric Clouds," Applied Optics, v. 12, n. 10, p. 2401-2414, October 1973.
16. Kennedy, R.S., "Communication Through Optical Scattering Channels: An Introduction," Proceedings of the IEEE, v. 58, n. 10, p. 1651-1665, October 1970.
17. Kennedy, E.A., personal communication.
18. Yarif, A., Introduction to Optical Electronics, 2d. ed., Holt, Rinehart and Winston, p. 306-307, 1976.
19. Ault, E.R., Bradford, R.S., Jr., and Bhaumik, M.L., "High-Power Xenon Fluoride Laser," Applied Physics Letters, v. 27, p. 413, 1975.
20. Laser Focus, v. 13, p. 32-33, September 1977.
21. Naval Research Laboratory Report 4031, Horizontal Attenuation of Ultraviolet and Visible Light by the Lower Atmosphere, by L. Dunkelmann, p. 7-10, 13, 17, 19, and 21, 10 September 1952.
22. Penndorf, R., "Tables of the Refractive Index for Standard Air and the Rayleigh Scattering Coefficient for the Spectral Region Between 0.2 and 20.0 μ and Their Application to Atmospheric Optics," Journal of the Optical Society of America, v. 47, n. 2, p. 179, February 1957.

23. Aeronautical Research Associates of Princeton Report 314, Ultraviolet Single Scattering Phase Function of Naturally Occurring Atmospheric Aerosols, by M.E. Neer, J.M. Schlupf, and P.C. Petersen, September 1977.
24. Zachor, A.S., "Aureole Radiance Field About a Source in a Scattering-Absorbing Medium," submitted for publication.
25. Pratt, W.K., Laser Communication Systems, p. 177-178, John Wiley & Sons, Inc., 1969.
26. Ross, M., Laser Receivers, John Wiley & Sons, Inc., 1966.
27. Gagliardi, R.M. and Karp, S., Optical Communications, John Wiley & Sons, 1976.
28. Valley, S.L., Handbook of Geophysics and Space Environments, Air Force Cambridge Research Laboratories, Office of Aerospace Research, U.S. Air Force, p. 7-6, 1965. (Also published by McGraw-Hill Book Co., 1965)
29. Uros, N.M., personal communication.
30. RCA, Electro-Optics Handbook, p. 114-115, 1974.
31. Selby, S.M., Standard Mathematical Tables, 23d ed., p. 103-104, CRC Press, Inc., 1975.
32. Scripps Institution of Oceanography, Reference 71-1, Underwater Lighting by Submerged Lasers and Incandescent Sources, by S.Q. Duntley, June 1971.
33. Duntley, S.Q., Journal of the Optical Society of America, V. 53, p. 214, 1963.

INITIAL DISTRIBUTION LIST

	<u>AGENCY</u>	<u>NO. COPIES</u>
1.	Defense Documentation Center Cameron Station Alexandria, Virginia 22314	2
2.	Dr. Richard S. Hughes Naval Weapons Center China Lake, California	2
3.	Dr. Michael E. Neer Aeronautical Research Associates of Princeton, Inc. (ARAP) 50 Washington Road Princeton, New Jersey 08540	1
4.	Dr. Alexander S. Zachor Honeywell, Inc. Radiation Center 2 Forbes Road Lexington, Massachusetts 02173	1
5.	Associate Professor John P. Powers Code 62Po Department of Electrical Engineering Naval Postgraduate School Monterey, California 93940	1
6.	Library, Code 0142 Naval Postgraduate School Monterey, California 93940	2
7.	Office of Research Administration Code 012A Naval Postgraduate School Monterey, California 93940	1
8.	Department Chairman, Code 61 Department of Physics and Chemistry Naval Postgraduate School Monterey, California 93940	2
9.	Professor William M. Tolles, Code 61T1 Department of Physics and Chemistry Naval Postgraduate School Monterey, California 93940	40
10.	LT Dennis M. Junge 2705 N. Prospect Colorado Springs, Colorado 80907	2

27422

Thesis
J964
c.1

Junge

Non-line-of-sight
electro-optic laser
communications in the
middle ultraviolet.

272872

27422

Thesis
J964
c.1

Junge

Non-line-of-sight
electro-optic laser
communications in the
middle ultraviolet.

172872

thesJ964

Non-line-of-sight electro-optic laser co



3 2768 002 11476 1
DUDLEY KNOX LIBRARY